Hydrazone analogs as DNA gyrase inhibitors and antioxidant agents: Structure-activity relationship and pharmacophore modeling

Ouafa Dammene Debbih, Wissam Mazouz, Ouided Benslama, Bachir Zouchoune, Ilhem Selatnia, Rafika Bouchene, Assia Sid, Sofiane Bouacida, Paul Mosset

Hydrazone analogs as DNA gyrase inhibitors and antioxidant agents: structure-activity relationship and pharmacophore modeling

Ouafa Dammene Debbih [1, *], Wissam Mazouz [2], Ouided Benslama [2, 3], Bachir Zouchoune [4, 5], Ilhem Selatnia [1], Rafika Bouchene [6], Assia Sid [1], Sofiane Bouacida [5, 6] and Paul Mosset [7]

[1] Laboratoire des Sciences Analytiques, Matériaux et Environnement, Université d'Oum El Bouaghi, Oum El Bouaghi 04000, Algérie ;
[2] Département des Sciences de la Nature et de la Vie, Faculté des Sciences Exactes et Sciences de la Nature et de la Vie, Université d'Oum El Bouaghi, Oum El Bouaghi 04000, Algérie ;
[3] Laboratoire de Substances Naturelles, Biomolécules et Applications Biotechnologiques, Université d'Oum El Bouaghi, Oum El Bouaghi 04000, Algérie ;
[4] Laboratoire de Chimie Appliquée et Technologie des Matériaux, Université d'Oum El Bouaghi, Oum El Bouaghi 04000, Algérie ;
[5] Unité de Recherche de Chimie de l'Environnement et Moléculaire Structurale, Université des frères Mentouri Constantine 1, Constantine 025000, Algérie ;
[6] Département des Sciences de la Matière, Faculté des Sciences Exactes et Sciences de la Nature et de la Vie, Université d'Oum El Bouaghi, Oum El Bouaghi 04000, Algérie ;
[7] Université de Rennes 1, Institut des Sciences Chimiques, CNRS UMR 6226, Avenue du Général Leclerc, 35042 Rennes Cedex, France.
* Corresponding author: dammenedebbih.ouafa@univ-oeb.dz
https://orcid.org/0000-0003-2757-4701

Abstract

In this paper, we report the synthesis and the structure–activity relationship study of three hydrazone analogs; the *Schiff* base hydrazone **SBH** and 2, 4-dinitrophenylhydrazones **H1** & **H2** derived from (*E)*-chalcones, to identify the active fragment of each structure. This identification has been carried out following in vitro biological evaluation, which revealed that the analogs **H1** and **H2** showed significant antibacterial activity, due to their (*E)*-chalcone fragments characterised by proton NMR data, and demonstrated by the docked view with emphasis on the involvement of these moieties in the interaction with the DNA gyrase, and thus contributes to the pharmacophore modeling. While **SBH** exhibited the highest free radical DPPH scavenging power that was associated to both hydrogen bonding and conjugated push–pull chromophores, which were elucidated by respectively; reported vibrational assignments and absorption spectra. The DFT optimizations gave rise to non-planar and distorted structures around the hydrazone group with comparable geometrical parameters. The chemical descriptors predict comparable biological activities, while the BDE necessary for the H-abstraction indicated a best antioxidant activity for the *Schiff* base hydrazone **SBH** compound.

Keywords: *Schiff* base; Hydrazones; Spectroscopic analysis; Biological activities; Bond dissociation energy; molecular docking.

Graphical abstract

SYNOPSIS : 2, 4-Dinitrophenylhydrazone analogs with (*E*)-chalcone and/or push-pull moieties were synthesized and characterized. The in-vitro and in-silico studies were carried out both to find the structure-activity relationship and to model the pharmacophore.

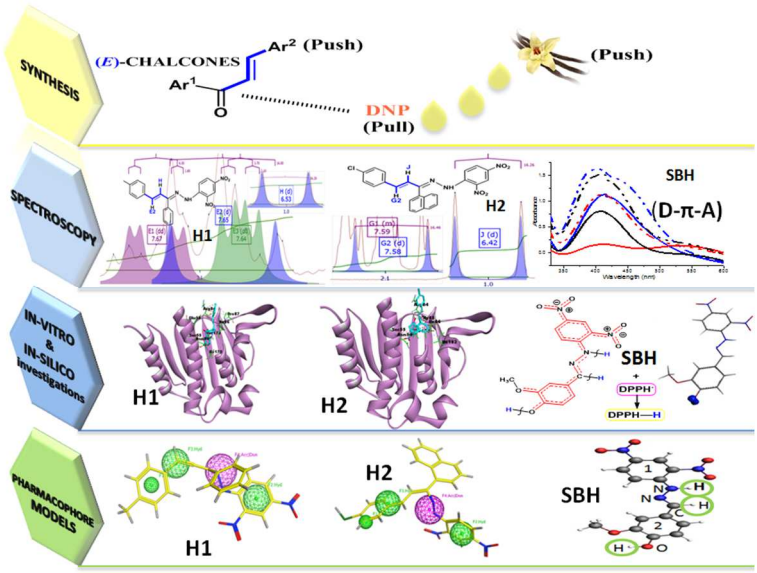

1 Introduction

Hydrazones and their derivatives with structure $R^1R^2C{=}NNR^3R^4$,[1] constitute an important and versatile class of compounds that have found great utility in organic synthesis.[2] In arylhydrazone products, the presence of an amino group with properties are similar to those of aromatic amines but having a more labile proton and lower toxicity make them promising antioxidants.[3] In addition, it is well known that the hydrazone group is known to play an important role in antimicrobial activity.[4–6]

Furthermore, *Schiff* base hydrazones are very widely used organic compounds. They have gained increasing interest in medicinal chemistry,[7] industrial and pharmaceutical fields due to the presence of an azomethine proton –N=CH–.[8–10] These compounds possess remarkable biological properties, such as antifungal, antibacterial, antimalarial, antiproliferative, anti-inflammatory, anticonvulsant, antiviral and antipyretic activities.[11–14] The anticancer potential of these compounds has also been investigated to some extent. Indeed, vanillin semicarbazone has shown pronounced anticancer properties.[15]

Due to the simplicity of their synthesis conditions, various chemical libraries can be designed to discover the potential of these molecules.[16]

In this work, the *Schiff* base hydrazone **SBH** was synthesized in the presence of vanillin (4-hydroxy-3-methoxybenzaldehyde) and DNP (2,4- dinitrophenylhydrazine). The latter was also the reagent for the synthesis of two analogs **H1** and **H2**, derived from *E*-chalcones. The structures of the products were characterised using FTIR, Raman, UV-vis, and ^{1}H & ^{13}C NMR. The antibacterial and antioxidant activities were evaluated. A DFT investigation using the chemical descriptors is employed to give an in-depth insight into the chemical reactivity and the antioxidant potency based on various research works.[17–19] This approach also aims to study the structure-activity relationship and identify pharmacophores potentially responsible for these activities. This was done through molecular docking study.

2 Experimental

2.1 General procedures and materials

Chemicals were purchased from Sigma-Aldrich and Carlo Erba. The melting point was measured on a Kofler bench and confirmed with a Barnstead Electrothermal BI 9100 digital device apparatus. Infrared spectra were performed with a Bruker-RAM II FT–IR spectrometer. The UV-Visible spectra were recorded on a SHIMADZU UV/Vis/NIR 16A spectrophotometer. The ^{1}H and ^{13}C NMR spectra were obtained in $CDCl_3$ and DMSO-d_6 on a Brüker Avance III (500/300 MHz for ^{1}H and 100/75 MHz for ^{13}C) using TMS as an internal standard. The in vitro anti-radical activity test was carried out by determining the ability to scavenge the free radical DPPH, using a Spectronic Unicam type as a monochromatic spectrophotometer.

2.2 SBH, H1 and H2 hydrazone analogs Synthesis

The synthesis of hydrazones **H1** and **H2** starts with the preparation of (*E*)-chalcones **C1** and **C2**; (*E*)-1-phenyl-3-(p-tolyl)prop-2-en-1-one and (*E*)-3-(4-chlorophenyl)-1-(naphthalen-1-yl)prop-2-en-1-one, respectively, by mixed aldol reaction of equimolar aromatic ketones and substituted benzaldehydes (Scheme 1). These carbonyl products serve as intermediates in the next step.

For the synthesis of the 2,4-dinitrophenylhydrazone derivatives **SBH**, **H1** and **H2**, the procedure described in reference[20] was used

To an acidic solution of DNP (**2**) (Brady's reagent[21] prepared by carefully adding a few drops of concentrated sulfuric acid to a suspension of 2,4-dinitrophenylhydrazine in 10 mL of methanol), an ethanolic solution of chalcones **C1**, **C2** or vanillin (**1**) was gradually added. The equimolar mixture consisting of 0.7 mmol of the latter and of DNP, was kept under stirring and heating at reflux (90-100 °C) for about 7-11 hours. The progress of the reaction (Scheme 1) was monitored by TLC until the disappearance of the reagents.

The hydrazone precipitated from each reaction was isolated by filtration; after allowing the reaction mixture to cool at room temperature, it was washed with ethanol and purified by recrystallization from ethanol.

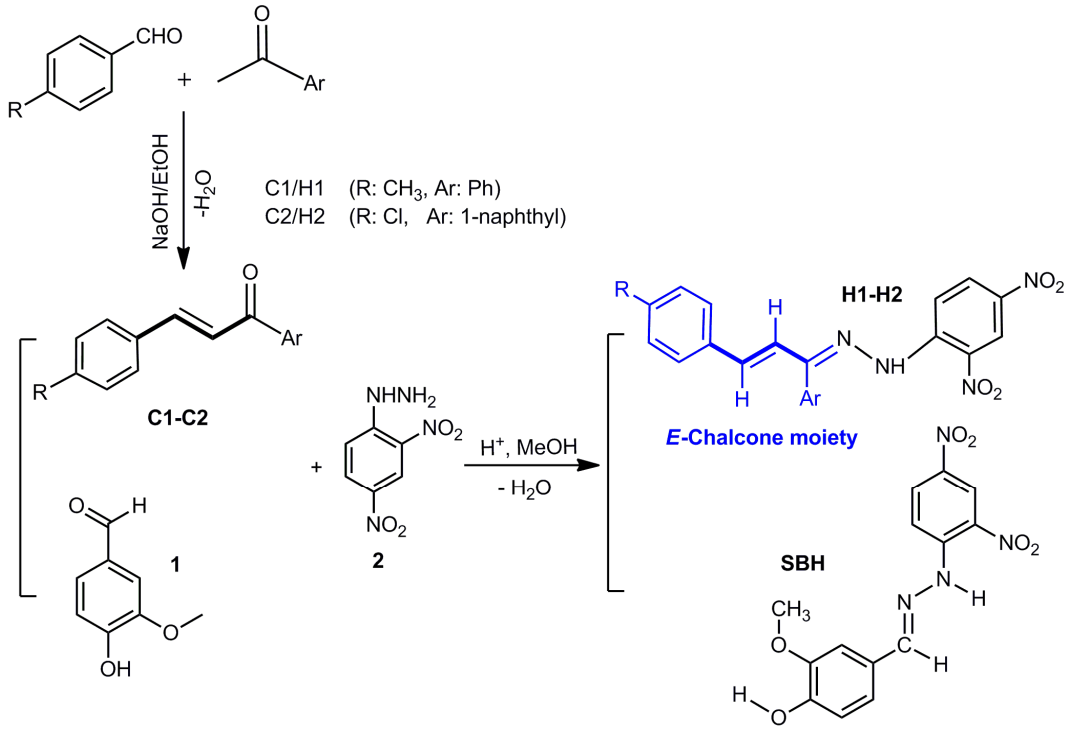

Scheme 1. Synthesis of SBH, H1 and H2 hydrazone analogs.

Analytical data of SBH

(E)-4-((2-(2,4-dinitrophenyl)hydrazono)methyl)-2-methoxyphenol **:** Red powder (yield 93.9%, m.p. 272-273 °C); IR *(υ, cm^{-1}) :* 3308-3388 (O–H), 3272 (N–H), 3076-3112 (C–H sp^2), 2974 (C–H sp^3), 1590 (C=N), 1489-1542 (C=C aromatic), 1453 (N–H), 1386 (N–O), 1257 (C–O); UV *(λ_{max}, nm) :* 228, 308, 389 ($\pi\rightarrow\pi^*$) in CH_2Cl_2 ; ^{1}H NMR *(300 MHz, DMSO-d_6, δ ppm, J Hz):* δ 11.57 (s, 1H), 9.71 (s, 1H), 8.85 (d, J = 2.6 Hz, 1H), 8.56 (s, 1H), 8.34 (dd, J = 9.7; 2.7 Hz, 1H), 8.08 (d, J = 9.7 Hz, 1H), 7.39 (d, J = 1.9 Hz, 1H), 7.17 (dd, J = 8.2;

1.9 Hz, 1H), 6.87 (d, *J* = 8.1 Hz, 1H), 3.86 (s, 3H); ^{13}C NMR *(75 MHz, DMSO-d_6, δ ppm) :* δ 150.20, 149.62, 148.16, 144.68, 136.51, 129.65, 128.97, 125.25, 123.13, 122.62, 116.75, 115.62, 109.61, 55.68.

Analytical data of H1

(Z)-1-(2,4-dinitrophenyl)-2-((E)-1-phenyl-3-(p-tolyl)allylidene)hydrazine **:** Orange–red crystals (yield 92%, m.p. 179 °C); IR *(υ, cm^{-1})*: 3275 (N–H), 3027-3095 (C–H sp^2), 2915 (C–H sp^3), 1611 (C=N), 1587 (C=C alkene), 1492-1518 (C=C aromatic), 1444 (N–H), 1364 (N–O); UV *(λ_{max}, nm)*: 233, 25, 305, 400 (π→π*) in CH_2Cl_2; ^{1}H NMR *(500 MHz, $CDCl_3$, δ ppm, J Hz)*: δ 11.11 (s, 1H), 9.06 (d, *J* = 2.6 Hz, 1H), 8.34 (dd, *J* = 9.6; 2.6 Hz, 1H), 8.11 (d, *J* = *9.6* Hz, 1H), 7.70-7.63 (m, 3H), 7.38-7.31 (m, 4H), 7.21-7.13 (m, 3H), 6.53 (d, *J* = 16.2 Hz, 1H), 2.36 (s, 3H); ^{13}C NMR *(100 MHz, $CDCl_3$, δ ppm)*: δ 154.57, 144.89, 143.02, 140.79, 139.29, 136.64, 132.36, 130.34, 130.19, 130.03, 129.74, 128.96, 128.75, 127.67, 123.68, 116.91, 115.60, 21,63.

Analytical data of H2

(Z)-1-((E)-3-(4-chlorophenyl)-1-(naphthalen-1-yl)allylidene)-2-(2,4-dinitrophenyl) hydrazine **:** Orange crystals (yield 57.9%, m.p. 265°C); IR *(υ, cm^{-1})* : 3267 (N–H), 3005-3097 (C–H sp^2), 1612 (C=N), 1590 (C=C alkene), 1506-1516 (C=C aromatic), 1489 (N–H), 1362 (N–O); UV *(λ_{max}, nm)* : 229, 271, 305 399 (π→π*) in CH_2Cl_2; ^{1}H NMR *(300 MHz, $CDCl_3$, δ ppm, J Hz)*: δ 10.81 (s, 1H), 8.97 (d, *J* = 2.5 Hz, 1H), 8.35 (ddd, *J* = 9.6 ; 2.6 ; 0.8 Hz, 1H), 8.18-8.10 (m, 2H), 8.03 (dd, *J*=7.9; 1.3 Hz, 1H), 7.72 (dd, *J* = 8.3 ; 7.0 Hz, 1H), 7.63-7.55 (m, 2H), 7.52-7.41 (m, 3H), 7.36-7.27 (m, 4H), 6.42 (d, *J* = 16.3 Hz, 1H); ^{13}C NMR *(75 MHz, $CDCl_3$, δ ppm)* : δ 156.51, 144.07, 138.39, 137.67, 135.05, 134.55, 134.25, 131.10, 130.05, 129.87, 129.75, 129.31, 129.19, 128.59, 128.53, 127.97, 127.32, 127.04, 126.02, 124.49, 123.48, 116.58.

2.3 Biological activity

2.3.1 Antibacterial test procedure

The antibacterial activity of the nitrogenous synthesized products **H1**, **H2** and **SBH** was carried out using the agar disk diffusion method;[22] against *Escherichia coli*, *Staphylococcus aureus* and *Pseudomonas aeruginosa*. The concentration range of the solutions prepared in DMSO was: 0.5; 1; 2; 4 and 8 mg/mL.

2.3.2 Antioxidant test procedure

The determination of the free radical scavenging capacity of each solution of the three synthesized compounds **H1**, **H2** and **SBH** in DMSO,[23] was measured according to the method described in references[24, 25].

2.4 Computational methods

Density functional theory (DFT) calculations were performed in water using the Amsterdam Density Functional (ADF.2021) program[26] developed by Baerends and co-workers[27–31]. The electron correlation was treated within the Local Density Approximation (LDA) in the Vosko-Wilk-Nusair parametrization.[32] All studied structures were optimized at the hybrid-type B3LYP functional (Becke's three-parameter hybrid exchange functional coupled with the Lee-Yang-Parr non-local correlation functional).[33, 34] The numerical integration procedure used for the calculations was developed by te Velde et al.[31]. The atom electronic configurations were described by a triple-z Slater-type orbital (STO) basis set for H 1s, C 2s and 2p, O 2s and 2p, N 2s and 2p, and Cl 3s and 3p augmented with a 3d single-ζ polarization for C, O, N and Cl atoms and with a 2p single-ζ polarization for H atoms. Full geometry optimizations were carried out using the analytical gradient method implemented by Versluis and Ziegler.[35] Frequency calculations[36, 37] were performed to confirm that the optimized structures are at local minima on the potential energy surface (PES). Representation of the molecular orbitals and molecular structures was done using ADF-GUI.[26]

The total enthalpy (***H***) of ArOH or ArNH compounds is calculated at the same level as that used for geometry optimizations and vibrational frequencies and is determined in conjunction with the equation below:

$$\boldsymbol{H} = \mathrm{E} + \mathrm{ZPE} + \Delta H_{\mathrm{trans}} + \Delta H_{\mathrm{rot}} + \Delta H_{\mathrm{vib}} + \mathrm{RT}$$

The BDEs (bonding dissociation enthalpies) are obtained from ΔH_{298}, taking into account the ZPE (Zero Point Energy) and the contributions of the translational ($\Delta H_{\mathrm{trans}}$), rotational ($\Delta H_{\mathrm{rot}}$) and vibrational ($\Delta H_{\mathrm{vib}}$) degrees of freedom in the heat of reaction at 298 K. These are the standard temperature correction terms calculated using equilibrium statistical mechanics with the harmonic oscillator and rigid rotor approximations. The BDEs at 298 K, 1 atm are calculated as follows using the method adopted in previous works:[38, 39]

BDE = $[\{\boldsymbol{H}(\mathrm{ArO}^{\bullet}) + \boldsymbol{H}(\mathrm{H}^{\bullet})\} - \{\boldsymbol{H}(\mathrm{ArOH})\}]$ for H-abstraction of O–H with regard to the hydrogen atom transfer mechanism: $\mathrm{ArOH} + \mathrm{R}^{\bullet} \rightarrow \mathrm{Ar–O}^{\bullet} + \mathrm{R–H}$.

BDE = $[\{\boldsymbol{H}(\mathrm{ArN}^{\bullet}) + \boldsymbol{H}(\mathrm{H}^{\bullet})\} - \{\boldsymbol{H}(\mathrm{ArNH})\}]$ for H-abstraction of N–H with regard to the hydrogen atom transfer mechanism: $\mathrm{Ar–NH–N{=}CH–Ar} + \mathrm{R}^{\bullet} \rightarrow \mathrm{Ar–N}^{\bullet}\mathrm{–N{=}CH–Ar} + \mathrm{R–H}$.

The solvent effect using the Conductor-like Screening Model for Realistic Solvent (COSMO-RS) developed by Klamt and co-workers[40] was introduced in the single point DFT

calculations, where the Cartesian coordinates were extracted from the geometry optimizations.

2.5 Molecular Docking study

In complement to the in vitro evaluation of the **SBH**, **H1**, and **H2** antibacterial activity, a molecular docking analysis of the inhibitory activity of these three compounds against the bacterial enzyme DNA-gyrase was carried out. The 3D structure of the targeted enzyme was downloaded from the PDB (Protein Data Bank) database (https://www.rcsb.org/) with the identifier ID: 4URO. The 3D structure of the enzyme resolved by the X-Ray diffraction method with a resolution of 2.59 Å, includes the *S. aureus* DNA gyrase subunit B in complex with the antibiotic Novobiocin co-crystallized in the ATP-binding site pocket of the enzyme. The 3D structure of the target protein was prepared for the molecular docking process by the Chimera 1.05 program, where a first step of purification of the structure was carried out by removing all solvents and water molecules. The hydrogen atoms and Gasteiger charge were then added and the final structure was saved in Mol2 format. On the other hand, the cif format of the molecules **H1** and **H2**, along with the cdx format of **SBH** have been converted to Mol2 format using the Open Babel program. The total energy of the three analogues has been minimized for their molecular docking. The molecular docking procedure was carried out using the Autodock Vina program, known for its precision and speed.[41] To validate the docking process, the structure of the antibiotic Novobiocin was retrieved from the PubChem database (https://pubchem.ncbi.nlm.nih.gov/) and used in a preliminary docking step at the level of the same geometric site where the co-crystallized ligand is located. The Root-Mean-Square Deviation (RMSD) value between the two co-crystallized and docked ligands was calculated to estimate the degree of precision of the docking process used in this study. The binding energy obtained from Novobiocin was used as a reference, and only the compounds with scores lower than this reference have been considered as potential inhibitors of the biological activity of DNA gyrase.

2.5.1 Drug-likeness and ADMET profiling

The Drug-likeness and ADMET (absorption, distribution, metabolism, and excretion) profiling of the three synthetic molecules **SBH**, **H1** and **H2** were in silico evaluated based on

different biological and physicochemical parameters, in particular the validation of the Lipinski rule of five, Viber and Ghose rules using the online program SwissADME (http://www.swissadme.ch/index.php). In addition, the toxicological behavior of the three compounds was studied using the ADMETLab2.0 program (https://admetmesh.scbdd.com/) to analyze some important criteria such as carcinogenicity, mutagenicity, cardiotoxicity, and hepatotoxicity.

2.5.2 Pharmacophore modeling

A pharmacophore can be defined as a molecular model that describes the spatial correlation of ligand functional elements. Once created, the model can be used to test the inhibitory performance of a chemo library against a specific target.[42] Different pharmacophoric features with specific biological activity can construct a pharmacophore, including hydrogen donors/acceptors, hydrophobic atoms, and aromatic rings.[42] In this study, the pharmacophore model was generated from **H1** and **H2** using MOE 2015.10 software. Both compounds were energy-minimized using MMFF94x force field and were used for the construction of a training set database. Then, their functional features were aligned to generate common feature pharmacophore models using the Polarity-charge-hydrophobicity (PCH) scheme tool. Finally, the best model with the lowest RMSD value has been selected.

3 Results and discussion

3.1 Spectroscopic analysis

FT-IR, and UV-Vis spectra were plotted using OriginPro 9.0 SR2 software,[43] while ^{1}H NMR spectroscopic data were processed using MestReNova software (Mestrelab research) version: 12.0.2- 20910.[44]

3.1.1 Vibrational assignments

Analysis of the infrared spectrum of the **SBH** *Schiff* base sample (Figure 1); reveals that the (CH=N) stretching vibration was observed between 3076 and 3112 cm^{-1}.[45] The presence of the absorption band at 1590 cm^{-1} is characteristic of the imine group (C=N); which turns out to be relatively low in frequency compared to those in **H1** and **H2** infrared spectra (1611 and 1612 cm^{-1}, respectively) (Figure 1), means that the (C=N) nitrogen could form a strong

intermolecular hydrogen bond;[46] with a proton-donating azomethine, amino and/or hydroxy groups of the **SBH** structure. It is also supported by the formation of an intramolecular hydrogen bond between the imine nitrogen and the aromatic (dinitrophenyl) carbon atom as acceptor and donor of a proton, respectively.

In addition, Fig. 1 shows absorption bands appearing around 3272 cm^{-1} and in the interval 3308-3388 cm^{-1}, which can be attributed to (N–H) and (O–H) stretching vibrations in SBH, respectively. However, the broad (O–H) absorption band confirms our postulate about the presence of an intramolecular hydrogen bonding,[47] which contributed to improve the antioxidant potential by enhancing the π-delocalization in the aromatic ring;[48, 49] according to the structure-activity relationship study mentioned in section (**3.3**).

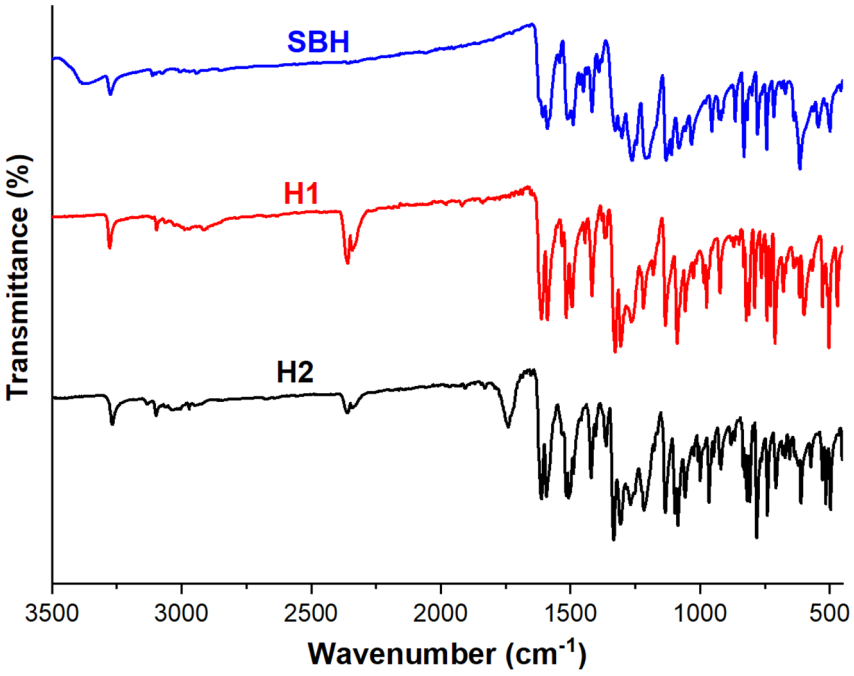

Figure 1. Infrared spectra of SBH, H1 and H2 synthesized hydrazones.

3.1.2 Electro-absorption spectra and solvatochromic behavior

In the electronic absorption spectra of synthesized **SBH** (Figure 2A & B); recorded in dichloromethane and ethyl acetate (0.5×10^{-4} M), the most intense band is located in the short-wavelength region whose maximum is at 228 nm in CH_2Cl_2 and 252 nm in AcOEt, corresponding to the π→π* transition associated with aromatic rings.[50]

Despite the weak π-delocalization of the phenylhydrazone moiety in the *Schiff* base structure, it gives rise to a band characterized by a very little hypsochromic effect of ~ 5 and 4 nm in previous solvents in the same order, compared to the corresponding band in the **H1** and **H2** absorption spectra, respectively. This may indicate the participation of non-bonded electron pairs of both hydroxyl and methoxy electron donating auxochromes in the mesomeric effect in this molecule.

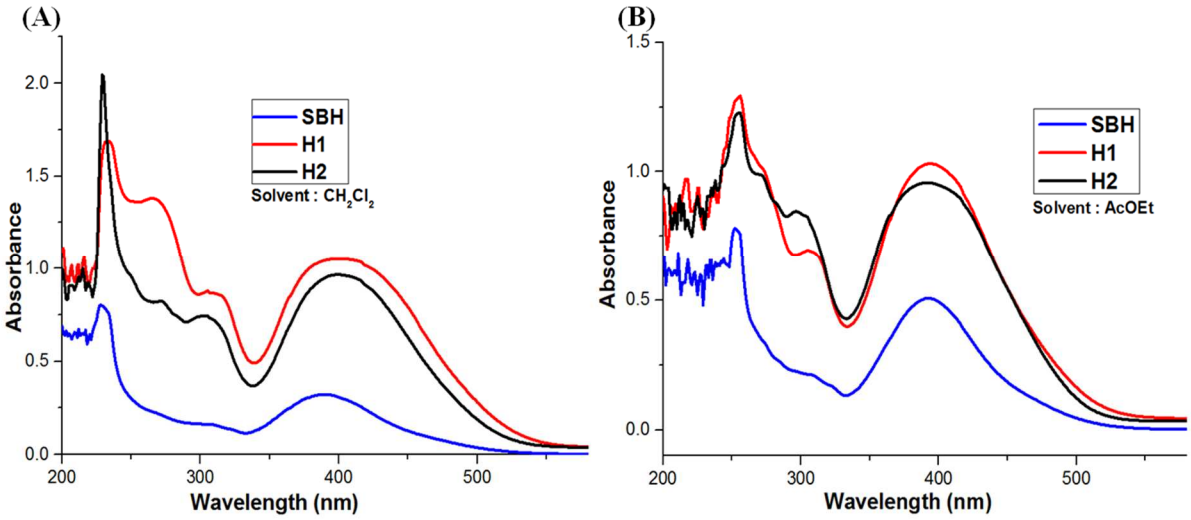

Figure 2. UV-Visible spectra of SBH, H1 and H2 (A) in CH_2Cl_2 (0.5×10^{-4} M); (B) in AcOEt (0.5×10^{-4}. M).

Furthermore, Fig. 2A & B shows large long wavelength absorption bands between 399 - 400 nm in CH_2Cl_2 and 392 - 394 nm in AcOEt, associated with the intramolecular charge transfer (ICT) character in 2, 4-dinitrophenylhydrazone-based donor-acceptor analogs.

However, the push-pull chromophores in the pi-conjugated **H1, H2** and **SBH** structures are characterized by different strengths and orientations, which are reflected in the positions of the absorption bands relative to each other. Indeed, the corresponding band in the absorption spectrum of the *Schiff* base hydrazone **SBH** is blue-shifted in CH_2Cl_2 and AcOEt (0.5×10^{-4} M) (Figure 2A & B), but shows a bathochromic effect in DMSO (25µg/mL) as follows (408.5 nm : **H2**, 411.5 nm : **H1** and 416 nm : **SBH**) (Figure 3), compared to those associated with **H1** and **H2**; this is due to the (D-π-A) arrangement in which the ICT complex originates from the hydroxyl and methoxy electron donor groups and extends to the two electron-withdrawing nitro groups of the **SBH** structure. Thus, the electronic excited state exhibits a higher stabilization in the polar aprotic solvent (DMSO) in the visible region.

In addition, the absorption bands attributed to the (D-π-A) transition of the ICT chromophores of the three synthesized 2,4-dinitrophenylhydrazone analogs are red-shifted towards the visible region with increasing solvent polarity, reaching maxima from 400 to 416 nm in DMSO at 25 and 50µg/mL; as can be seen in Figures 2 A & B and 3. These results show that DMSO is the suitable solvent that can promote the kinetics of the reaction between the DPPH radical and the antioxidant,[51] resulting in a radical R'• (Scheme 2); which can be stabilized by π-electron delocalization.

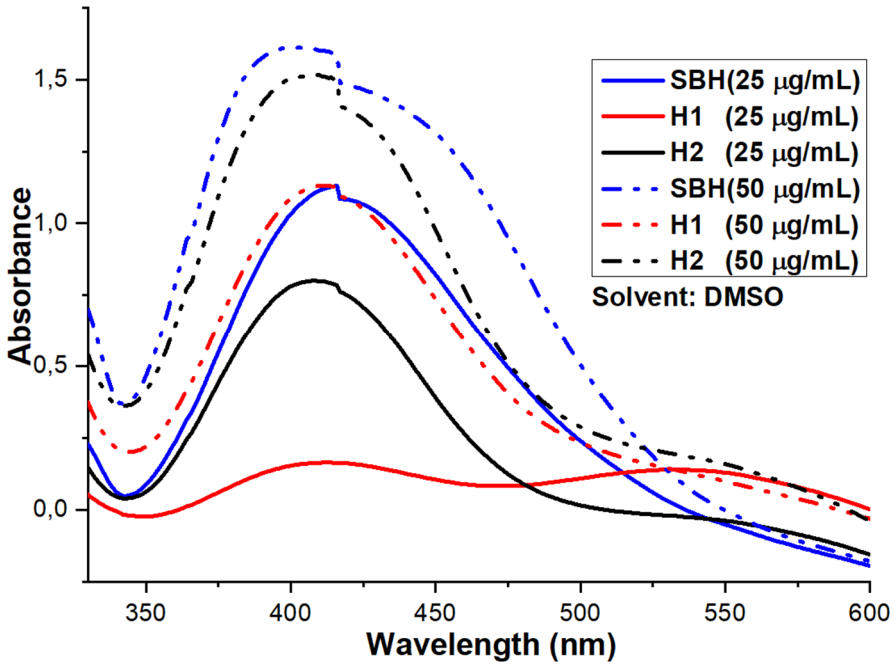

Figure 3. Absorption bands attributed to the electronic (D-π-A) transition of SBH, H1 and H2.

3.1.3 ^{1}H NMR spectroscopic analysis

The ^{1}H NMR spectrum of the *Schiff* base; 4-((2-(2,4-dinitrophenyl) hydrazono) methyl)-2-methoxyphenol **SBH** recorded in DMSO-d_6 (Figure 4), shows two singlets shifting to the weak field at δ= 11.57 and 9.71 ppm, attributed to the OH and NH protons, respectively. On the other hand, the protons of the methoxy group resonate as a 3H integrating singlet at 3.86 ppm. It has been reported that a methoxy substitution at the ortho-position relative to the hydroxyl significantly increases the antioxidant efficacy.[52]

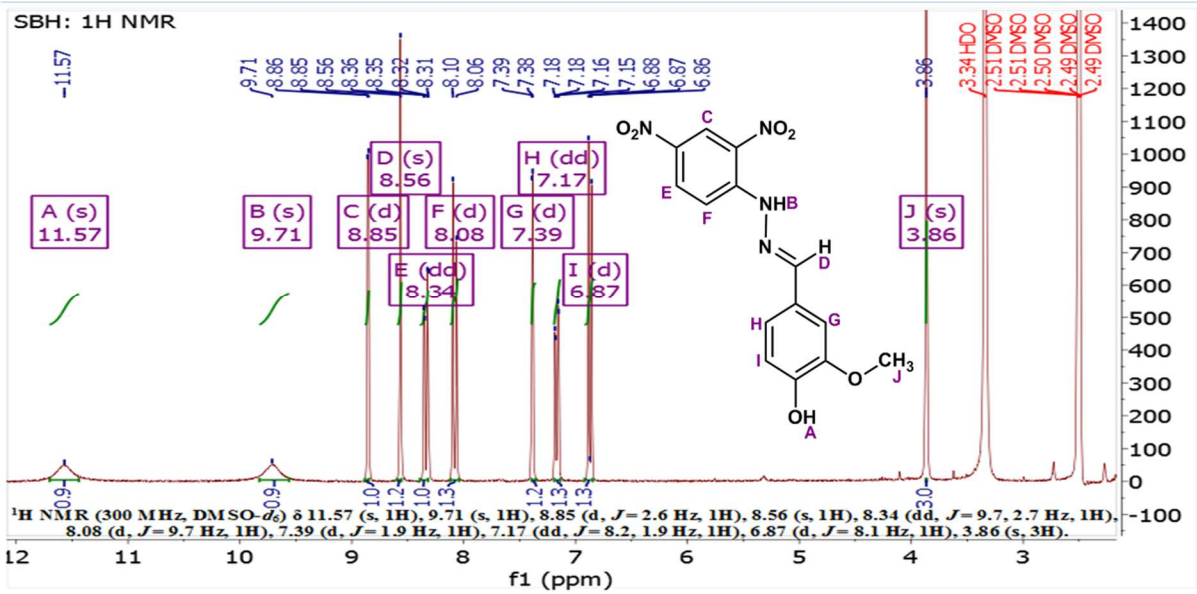

Figure 4. ^{1}H NMR spectrum of the synthesized hydrazone SBH in DMSO-d_6.

While the ^{1}H NMR spectra of **H1** (Figure 5A) and **H2** (Figure 6A) in $CDCl_3$ show that the proton of the NH group resonates at δ =11.11 and 10.81 ppm (singlets) for **H1** and **H2**, respectively.

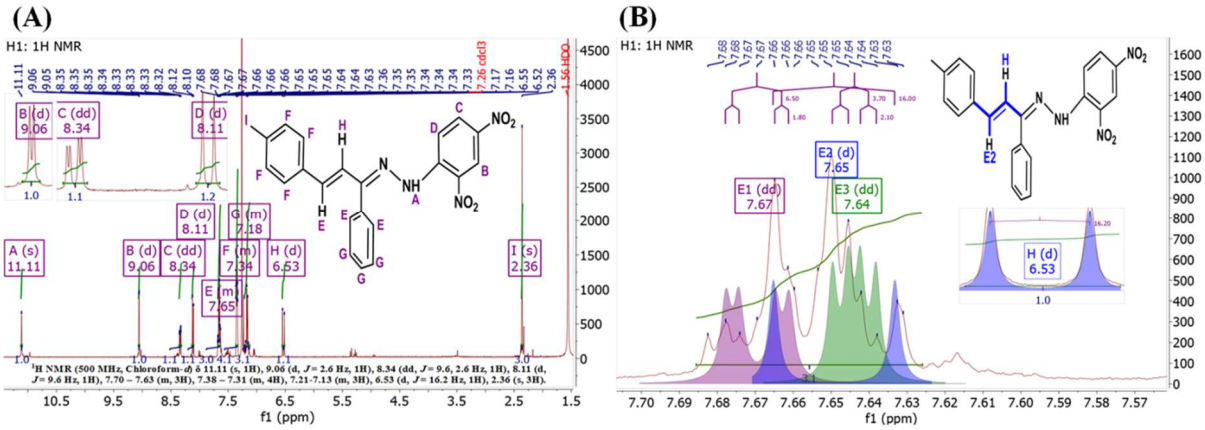

Figure 5. (A) ^{1}H NMR spectrum of H1 hydrazone in $CDCl_3$ (B) Simulated ^{1}H NMR spectrum of H1 hydrazone.

Figure 5A also reveals that the doublet at 6.53 ppm (J = 16.2 Hz) and the multiplet at around 7.70-7.61 ppm are attributed to the protons of the ethylenic group =CH of the **H1** hydrazone derivative. In order to find the coupling constants of the last signal, which has a rather

complex multiplicity, it was simulated and refined up to the theoretical/experimental superposition (Figure 5B). Indeed, the vinyl proton in question shows the same multiplicity (doublet) at 7.65 ppm,[53] with a coupling constant of the same order ($J \approx 16$ Hz). This value confirms the (*E)* stereochemistry of the double bond.[54]

However, Figure 6A & B of hydrazone **H2** indicates that the ethylenic protons resonate at around 6.42 ppm (d; J = 16.3 Hz) and 7.58 ppm (d; J = 16.5 Hz). The values of the coupling constants confirm the *E*-stereochemistry of the double bond, which is responsible for most biological activities.[55]

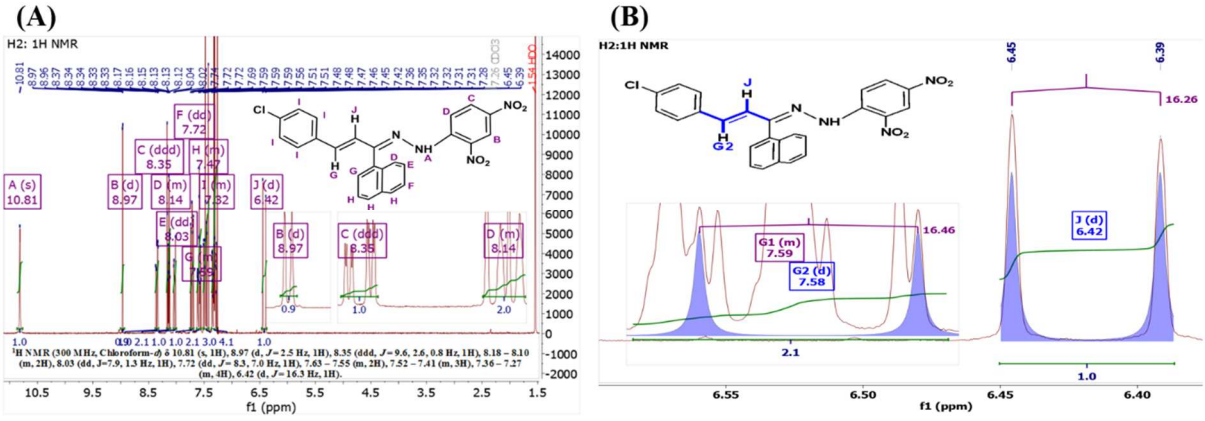

Figure 6. (A) ^{1}H NMR spectrum of H2 hydrazone in $CDCl_3$ (B) Simulated ^{1}H NMR spectrum of H2 hydrazone.

3.2 Quantum chemistry analysis

3.2.1 Optimized structures

The optimized structures of **H1**, **H2**, and **SBH** without symmetry constraints are shown in Figure 7. The common characteristic for all compounds is that they are built around the C=N–NH– hydrazone group and have a common part $(C_6H_4)(NO_2)_2(HN_2)$. In order to understand the origin of the modifications that occurred on the molecular structures and the electronic properties, the chemical bonding and electronic structures are discussed for all three compounds. Indeed, the structures sketched in Figure 7 show distorted structures around the hydrazone –HN–N=C group. The **SBH** structure is the less distorted with regard to the dihedral angle between the phenyl rings 1 and 2 which are oriented to each by less than 10°, whereas, the **H2** structure is the more distorted marked by dihedral angles of 25, 54, and 75°

between 1 and 3, 2 and 3 and 1 and 2 rings, respectively. However, the **H1** structure is moderately distorted, where the three rings are oriented to each by an angle of about 25°. In **H1**, **H2,** and **SBH** compounds the N–N and C=N bond distances of the hydrazone group are 1.368 and 1.297, 1.360 and 1.297 and 1.357 and 1.287 Å, respectively, are consistent with N–N single bond and C=N double bond in each case. These bond distances clearly show that the three structures are not sensitive to the substituents attached to the hydrazone group.

Moreover, the average C–C bond distances within the phenyl rings in all compounds are about 1.400 Å (Table 1), consistent with a bond order of 1.5, corresponding to delocalized π-systems as found in previous works[56–64], but somewhat longer than those encountered in the phenyl rings of about 1.392 Å, due to the electron-withdrawing effects of the NO_2 nitro groups attached to the phenyl ring 1. The B3LYP functional results reproduce well the experimental parameters for related compounds. Natural atomic populations[65] obtained by the NBO program[66, 67] have an important role in affecting dipole moment, molecular polarizability, electronic structure, basicity behavior, and so on. Indeed, the carbon atoms of sp^3 hybridization of methyl groups bore the most negative charges of -0.59, while the C(4) and C(7) carbon atoms of the 5-membered ring and phenyl ring 1, respectively, both attached to the –HN–N– group carry the most positive charges of +0.19 and +0.20, respectively.

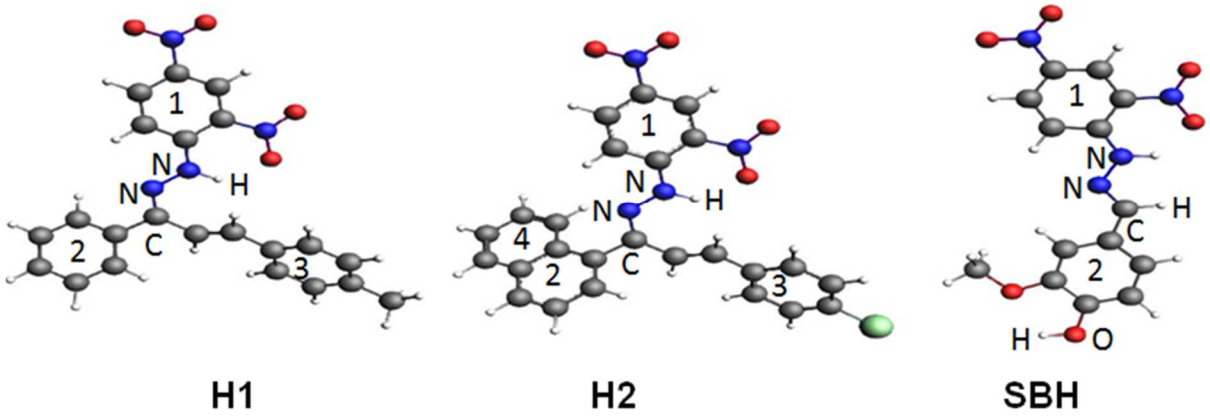

Figure 7. The lowest optimized structures of H1, H2 and SBH compounds. Atom colors: carbon (grey), oxygen (red), nitrogen (blue) chlorine (green) and hydrogen (white).

The natural populations have negative charges in the ranges -0.25 – -0.27 and -0.34 – -0.36 for the N(N=C) and N(NH) atoms belonging to the hydrazone, respectively, indicating that the hydrazone acts as a withdrawing group.

It is worth to note that the nitrogen atoms of each nitro NO_2 group linked to the phenyl ring carry the average charge of +0.57, due to their bonding to oxygen atoms with relatively large electronegativity attaining the average charge of -0.42. The MOs located in the vicinity of the HOMO and LUMO levels are plotted in Figure 8, separated by large HOMO-LUMO gaps of 3.03, 2.99, and 3.08 eV. The orbitals' energies are in accordance with their characters and their atomic localizations as shown in Figure 8. The HOMOs of the **SBH**, **H1**, and **H2** compounds are mainly localized on the C=N double bond of the hydrazone group, the carbon atoms of different phenyl exhibit $\pi_{C\text{-}C}$ bonding character and localized on the N atom of the hydrazone group corresponding to its lone pair. Based on the above discussion, the hydrazone group and the phenyl ring 2 could play a donor role, however, the phenyl ring 1 and the nitro groups play an acceptor role, by the nucleophilic and electrophilic characters, respectively. The HOMOs' and LUMOs' energies and their energy gap have a tight relationship with the chemical activity and kinetic stability of the molecules[68–71] and are used to determine the bioactivity from intramolecular charge transfer. The HOMO-LUMO gaps elucidate that the charge transfer interactions taking place within the **H1**, **H2**, and **SBH** compounds are responsible for the molecular reactivity.[68–71]

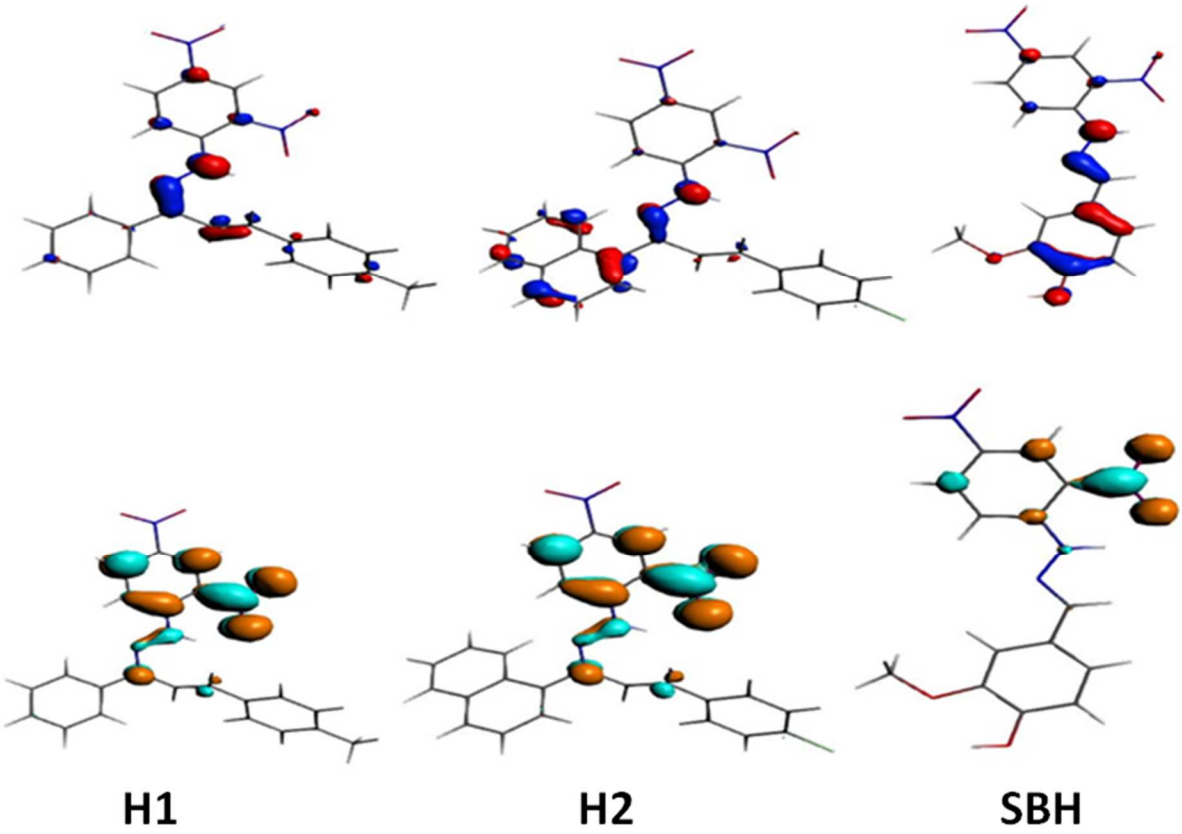

Figure 8. HOMOs (top) and LUMOs (bottom) for H1, H2 and SBH compounds. Contour values are of ±0.06 (e/Borh^3).

Table 1. Selected geometrical and energetic parameters of the H1, H2 and SBH compounds obtained by B3LYP, HOMO-LUMO gaps are in eV. The bond distances are given in Å and angles in (°).

	H1	**H2**	**SBH**
HOMO-LUMO gap (eV)	3.08	2.93	2.99
Bond length (Å)			
Average O-N (NO_2)	1.243	1.269	1.249
N-N	1.360	1.357	1.368
N-H	0.916	0.954	0.942
N-C ring 1	1.357	1.360	1.351
N-C (hydrazone)	1.297	1.297	1.287
Average C-C ring 1	1.402	1.401	1.400
Average C-C ring 2	1.395	1.406	1.396
Average C-C ring 3	1.396	1.394	-
Natural populations (NPA)			
Average N (NO2)	+0.54	+0.55	+0.56
N (N=C)	-0.26	-0.27	-0.25
N (N-H)	-0.35	-0.37	-0.36
Average O	-0.40	-0.41	-0.42

3.2.2 Molecular properties

The HOMO-LUMO gaps, the chemical hardness (η),[72, 73] the chemical potential (μ), and electrophilicity (ω)[74–76] as chemical descriptors are calculated in order to establish a comparative study in relation to their possible biological activities. These chemical descriptors are essential for the determination of the chemical stability and the chemical activity of molecular species.[68, 69]

Despite the slight differences obtained from the HOMO-LUMO gaps and the HOMOs' and LUMOs' energies, the values of electrophilicities in eV differ slightly obeying the increased order: **H1** (7.42) < **SBH** (7.64) < **H2** (7.95) as shown in Table 2.

The **H1**, **H2**, and **SBH** compounds could be recommended as a blood thinner in conjunction with their dipolar moment values of 7.88, 8.58, and 9.09 D (Table 2), respectively; following the same increased order as established for the electrophilicity indicating that **H1** is the less polarized inversely to **H2** which is the more polarized.

Values collected in Table 2 reveal that the global reactivity descriptors are sensitive to the substituents attached to the hydrazone group.

Table 2. The molecular properties (HOMO and LUMO energies, HOMO-LUMO gap, Ionization potential (IP), Electron affinity (EA), Chemical potential and electrophilicity in eV and the dipole moment in Debye) calculated for the H1, H2 and SBH compounds obtained by B3LYP functional. BDEs are given in kcal/mol and spin densities are in parentheses.

Molecular property	**H1**	**H2**	**SBH**
E_{HOMO}	-6.321	-6.328	-6.275
E_{LUMO}	-3.244	-3.392	-3.282
HOMO-LUMO gap	3.08	2.97	2.99
Ionization potential (IP)	6.321	6.328	6.275
Electron affinity (EA)	3.244	3.392	3.282
Chemical hardness (η)	1.54	1.485	1.495
Chemical potential (μ)	-4.7825	-4.860	-4.7785
Electrophilicity (ω)	7.42	7.95	7.64
Dipolar moment	7.88	9.09	8.58
	BDE and spin density		
N–H	66.3 (0.3775)	60.7 (0.3765)	62.7 (0.36)
O–H	-	-	59.3 (0.59)

3.3 Antibacterial and antioxidant test results & structure- activity relationship

The results of the in vitro antibacterial test, carried out by the disk diffusion method against the reference bacterial strains *Staphylococcus aureus*, *Pseudomonas aeruginosa,* and *Escherichia coli*; carried out on **SBH** hydrazone derived from vanillin, indicate that the latter has no activity. On the other hand, it has been observed that its analogs, especially **H2**; exhibit a significant activity against *E. coli* with a zone of inhibition that has reached 11 mm; for a concentration of 8 $mg.mL^{-1}$ in DMSO. This result is explained by the presence of a chalcone moiety in both **H1** and **H2**; known as an antibacterial agent in medicinal chemistry and showed up to sixfold stronger antibacterial activities than standard drugs on the market.[77, 78] Especially since these chalcones moieties have (*E*)-stereochemistry, as shown by our spectroscopic results of ^{1}H nuclear magnetic resonance; through the trans vicinal proton-proton coupling constant ${}^{3}j_{HH} \approx 16$ Hz of the vinyl group.[54] Indeed, as part of a large research program for new effective antimicrobial agents, it has been reported that a considerable number of (*E*)-chalcones have shown good antibacterial properties against *Staphylococcus aureus*, *Enterococcus faecali*s, and *Bacillus subtilis*.[79, 80]

However, the results of the antioxidant test carried out in the range of concentrations; 25, 50, 100, 200, 300, and 400 (µg/mL) (Table 3), using ascorbic acid as a reference, indicate that *Schiff* base hydrazone **SBH** has the freest radical scavenging activity (68.08%) with an IC_{50} = 269.55 µg/mL. That of ascorbic acid was 85.49 µg/mL, after 60 minutes of incubation in the dark. While **H1** and **H2** exhibit moderate antioxidant activity with a free radical inhibition percentage not exceeding 36.23 and 9.14% at a concentration of 50 and 400 µg/mL, respectively, and after the same incubation time.

Table 3. In vitro antioxidant activity of SBH and Standard after 60 mn.

Samples	Inhibition % at different concentrations (µg/mL)						**IC_{50} (µg/mL)**
	25	**50**	**100**	**200**	**300**	**400**	
SBH	8.24	12.76	22.61	42.20	57.80	68.08	**269.55**
As. Acid (Standard)	14.01	25.35	46.98	89.18	96.98	96.45	**85.49**

The values of (R^2) of the linear and logarithmic trend curves (Figure 9), respectively of the *Schiff* base 2, 4-dinitrophenylhydrazone **SBH** and the reference ascorbic acid are much more satisfactory than those of the test related to the 2, 4-dinitrophenylhydrazone **H1**-bearing chalcone reported by the reference[20]. This indicates a better agreement between the curve and the experimental data.

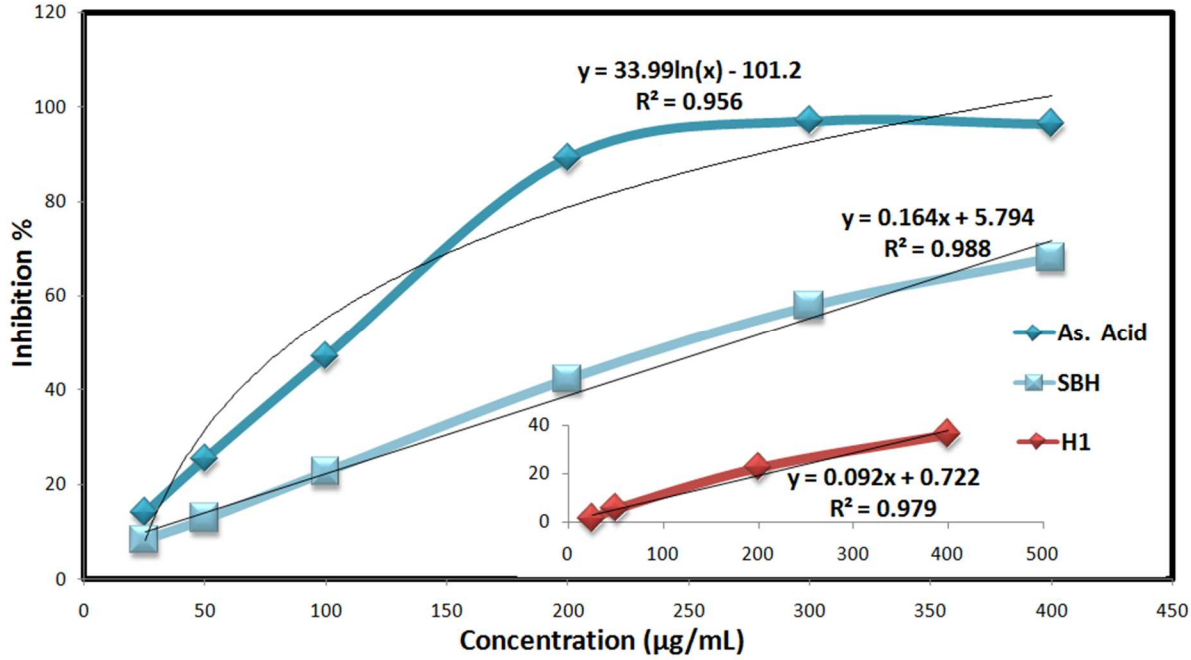

Figure 9. Antiradical activity of SBH, H1 hydrazones and standard ascorbic acid after 60 mn.

The scavenging of the free radical DPPH•; 2,2-diphenyl-1-picrylhydrazyl by the reducing agent (antioxidant) took place by a proton donation mechanism.[81, 82] The antioxidant ArOH or ArNH reacts with the free radical (DPPH•) by transferring a hydrogen atom to it. The DPPH• radical is more reactive than the resulting ArO• or ArN• radicals and which are usually stabilized by π-electron delocalization and hydrogen bonding.[83–87]

The results are in good agreement with the characterized structures of the three synthesized hydrazone analogs. Indeed, the proton donating ability of the N–H group in **H1**, **H2**, and **SBH** structures, and of the azomethine CH=N and O–H groups of the **SBH** structure gives a DPPH-H molecule (Scheme 2). In this case, the radical R'• (**H1**•, **H2**• or **SBH**•) arising from the electron transfer should also be stable, so that it does not react with the substrate molecules.[85] Thus, the antioxidant efficacy is all the greater the more stable this radical is.

The presence of the following parameters; the donor-acceptor system, the optimized electronic delocalization in DMSO solution (Fig. 3) and the formation of hydrogen bonds (as elucidated in the vibrational assignments section) in the studied hydrazone **SBH** structure, can contribute to promote the stability of its radical **SBH**•. However, the low antioxidant capacity of **H1** and **H2** stems from the presence of a single amino proton and probably from the steric hindrance of the naphthalene-1-yl moiety in the **H2** structure.

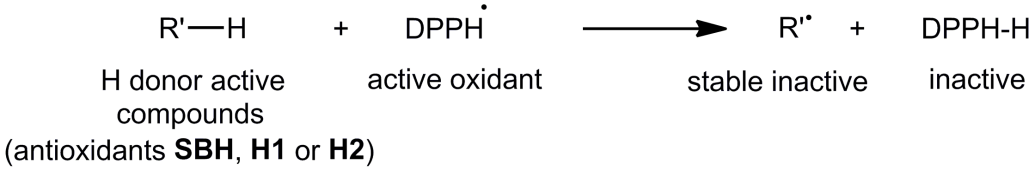

Scheme 2. Free radical DPPH• scavenging.

We were also interested in evaluating the H-abstraction from OH and NH of **SBH** and NH of **H1** and **H2** as shown in Figure 7. The determination of the antioxidant strength for **SBH**, **H1**, and **H2** is based on the BDEs of N–H or O–H bonds, the relative energies between the radicals formed, and the localization of the spin densities. The radicals formed after H-abstraction are noted **H1**•, **H2**•, **SBH**•(OH) and **SBH**•(NH). The **SBH**•(OH) radical obtained by H-abstraction from OH is 3.5 kcal/mol more stable than its analog **SBH**•(NH).

The difference in the antioxidant activity would be related to the π-electron delocalization, which leads to a stabilization of the radicals obtained after the H-abstraction. As mentioned earlier, the HOMO of **SBH** is localized on the phenyl ring bearing the alone OH group, which corresponds to the orbital containing the removed electron (Figure 8).

The lower the BDE value, the easier the dissociation of the O-H or N-H bond. To the phenolic H(O)– abstraction corresponds the weakest BDE's value of 59.3 kcal/mol giving rise to the most stable ArO• radical, which is computed as 3.4 kcal/mol more stable than ArN• obtained from the H(N)– abstraction. This weak energy difference suggests a competition between the two isomers, in relationship with the localization of the HOMO (Figure 8) encountered in **SBH**. The H(N)– abstraction leads to a relatively unfavorable radical with regard to BDE energies of the N–H bond breakage in the range 60-66 kcal/mol (Table 2), which are comparable to previous results of related compounds.[88]

The spin density values show that the unpaired electron is mainly located on the atom from which the H atom is extracted as summarized in (Table 2) and Figure 10.

The BDE values show that the H-transfer is more energetically preferred when the OH group is attached to the delocalized system like the C6 ring in only **SBH** compound.

The BDE values corresponding to the H-abstraction obey the decreasing order: N–H > O–H. It can be concluded that the weakest BDE energy matches up to the best relative antioxidant activity for **SBH**, while the largest energies correspond to the weak antioxidant activities for **H1** and **H2**.

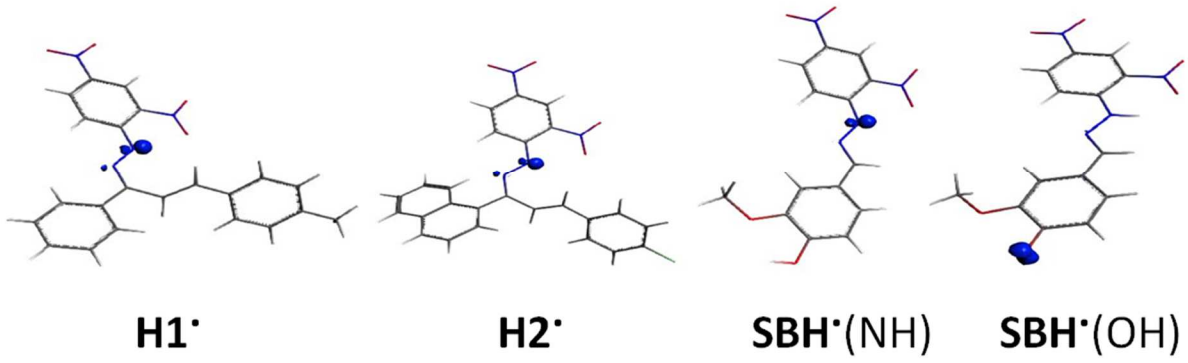

Figure 10. Spin density plots of H1, H2, SBH (NH) and SBH (OH) radicals.

3.4 Molecular Docking study

Compounds with antibacterial activity generally act by altering one of the key physiological elements of the bacterial cell, such as the proteins involved in cell wall synthesis, respiration, or DNA processing. Among the latter, the DNA gyrase is an enzyme of the topoisomerases class, that is responsible for the unwinding of the DNA molecule during the replication and transcription process. Being a component of the replisome complex, DNA gyrase is, therefore, crucial for bacterial survival and multiplication, which makes it an excellent target for new antibacterial drugs.[89] The virtual investigation approach is now considered complementary to experimental trialsof biological activity.[90] The molecular docking process has greatly contributed to the development of drug candidates that are used in the treatment of several diseases.[91] In view of this, a molecular docking investigation was carried out in order to understand the mode of binding and the types of molecular interactions established between the compounds **SBH**, **H1**, and **H2** and the active site gorge of DNA gyrase. This analysis provides a molecular basis for the inhibitory potential of these three compounds towards DNA gyrase, it is, therefore, essential for the design of drug candidates with

antibacterial activity.

The molecular docking was preceded by a validation step consisting of re-docking the co-crystallized ligandNovobiocin in the catalytic site of DNA gyrase. The RMSD score obtained by this procedure was 0.561A°, suggesting the precision of the molecular docking process. The reference ligand Novobiocin gave binding energy of -7.4 Kcal/mol and interacted with residues Asp81, Asn54, Arg144, Asp89, and Ser128 by forming hydrogen bonds and with Pro87, Ala98, Ile102, Arg84 by hydrophobic-bonding (Table 4). The **SBH**, **H1**, and **H2** analogs were docked in the same catalytic site and their binding affinity and bonding interactions are summarized in Table 4.

The obtained results revealed that the two synthesized compounds **H1** and **H2** show lower binding energies than Novobiocin, and they interact with at least one or more of the key active site residues of the target enzyme. The molecule **H1** exhibited the highest binding energy (-7.7 Kcal/mol) and is, therefore, considered to be the best inhibitor for the gyrase. On the other hand, the compound **H2** generates binding energy very close to that of **H1** with a value of -7.5 Kcal/mol.

The significant antibacterial activity of **H1** and **H2** may be explained by their strong interaction with the key amino acids of the active site by forming five hydrogen bonds with Thr173, Ser55, Gly85, Glu58, and Arg84 along with four hydrophobic bonds with Ile86, Asn54, Ile175,and Pro87 for compound H1 (Table 4, Figure 12). Whereas, **H2** interacts with Gly85, Thr173, Arg84, Glu58, and Ser55 by five hydrogen bonds and with Ile102, Ile86, and Asn54 by forming four hydrophobic interactions (Table 4, Figure 13). The molecule **H1** mediates also an electrostatic bonding with Arg84 and Glu58, which is similar to the interaction mode of the antibiotic Novobiocin (Table 4).

Table 4. Docking result of the co-crystallized, H1, H2, and SBH ligands within the active site of the gyrase enzyme.

	Binding energy (Kcal/mol)	Hydrogen interactions	Hydrophobic interactions	Van der Waals interactions	Electrostatic interactions
Novobiocin (co-crystallized)	-7.4	Asp81, Asn54, Arg144, Asp89, Ser128	Pro87, Ala98, Ile102, Arg84	Gln91, Gly85, Asp57, Thr173, Ser55, Gly125	Arg84, Glu58
SBH	-6.3	Gly85, Ser128, Gly125	-	Asp57, Asn54, Ser55, Asp81, Thr173, Glu58, Gly83, Pro87, Ile86,	-

				Ile102	
H1	-7.7	Thr173, Ser55, Gly85, Glu58, Arg84	Ile86, Asn54, Ile175, Pro87	Gly125, Asp57, Ile102, Val174, Ile51, Val79, Asp81, Gly85, Arg144	Arg84, Glu58
H2	-7.5	Gly85, Thr173, Arg84, Ser55, Glu58	Ile102, Ile86, Asn54	Gly125, Pro87, Ile175, Ile51, Asp81, Glu58, Gly83, Gly172, Asp57	-

The docked view of compounds **H1** and **H2** (Figures 12A and 13A) illustrates the good anchorage of these two analogs within the active site gorge of the gyrase. The view also shows the involvement of the **H1** and **H2** (*E*)-chalcone moieties in the interaction with the gyrase by forming hydrophobic binding, which reinforces the stability of the two complexes **H1**-gyrase and **H2**-gyrase. The mode of binding of the two analogs **H1** and **H2** may be the reason for their higher antibacterial potency observed in the in vitro assays, compared to the compound **SBH** which lacks the ability to form hydrophobic interactions with key residues of the gyrase catalytic site and exhibits binding energy of -6.3 Kcal/mol, less important than those of the other ligands (Table 4, Figure 11).

Finally, the results of the molecular docking analysis corroborate those obtained from the antibacterial activity tests carried out in vitro. It can be concluded that the two synthetic compounds **H1** and **H2** possess antibacterial activity by inhibiting DNA gyrase as a potential target.

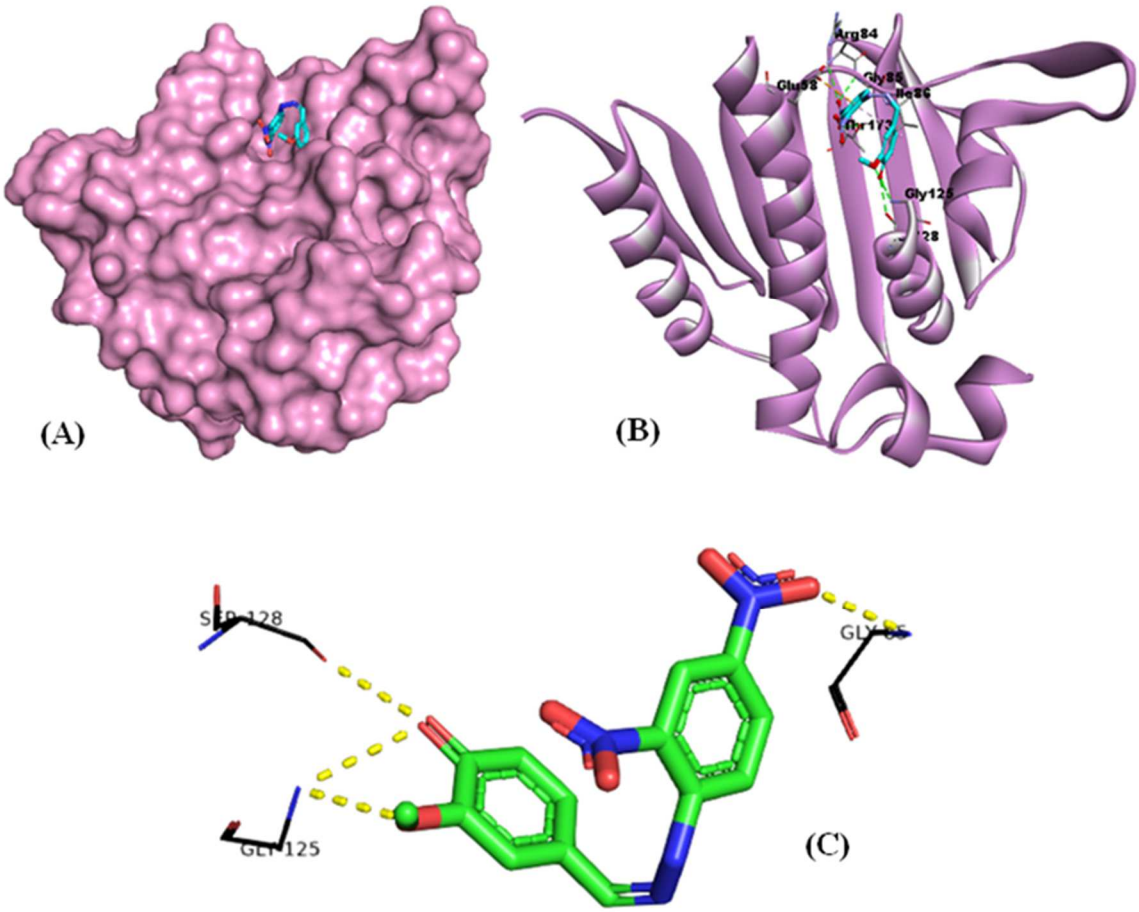

Figure 11. Predicted binding mode for SBH with gyrase. (A) View of the binding cavity, showing SBH as cyan sticks, bound to the surface of gyrase (4URO). (B) Profile view of SBH as cyan sticks bound in the gorge pocket of gyrase. Key residues for the binding of SBH are shown as green sticks. (C) 3D schematic diagram of docking model of SBH showing the hydrogen bonds formed with the gyrase active site.

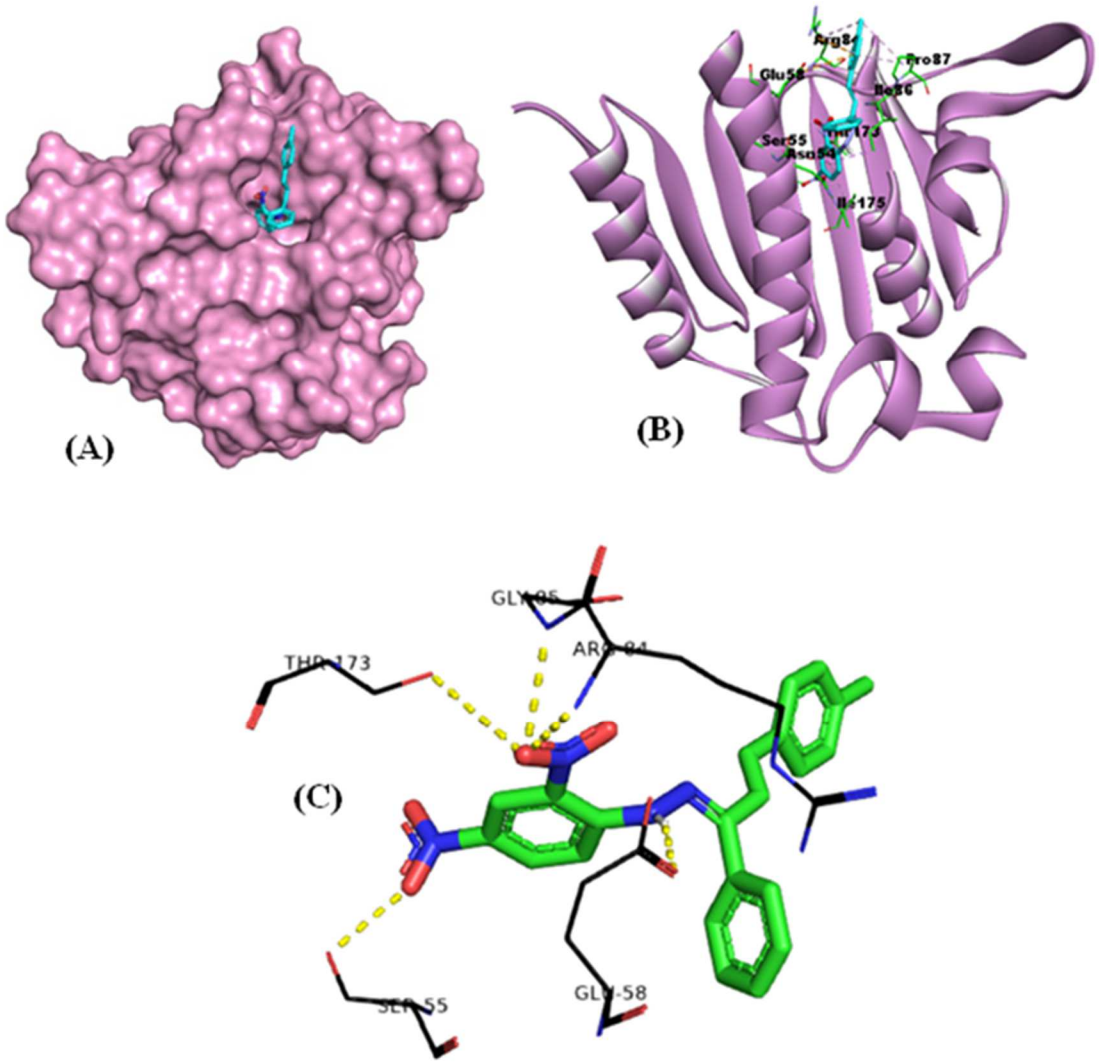

Figure 12. Predicted binding mode for H1 with gyrase. (A) View of the binding cavity, showing H1 as cyan sticks, bound to the surface of gyrase (4URO). (B) Profile view of H1 ascyan sticks bound in the gorge pocket of gyrase. Key residues for the binding of H1are shown as green sticks. (C) 3D schematic diagram of docking model of H1 showing the hydrogen bonds formed with the gyrase active site.

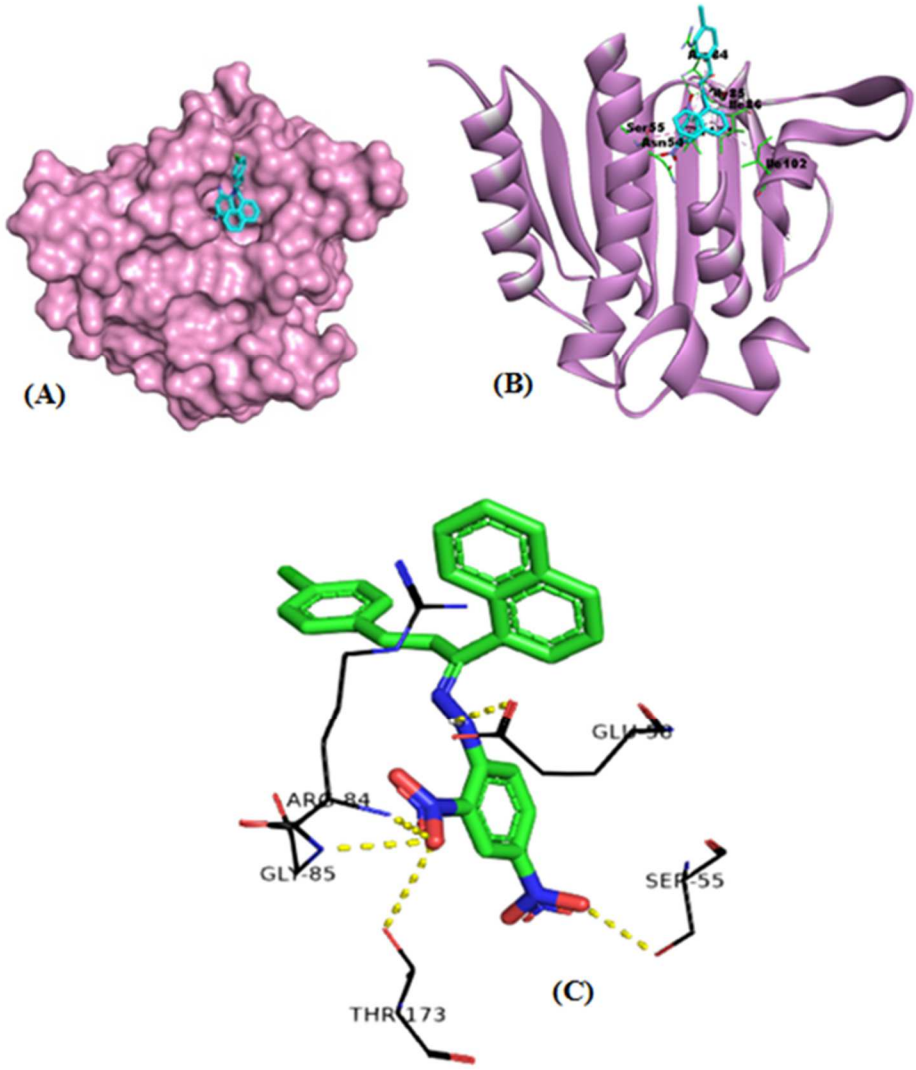

Figure 13. Predicted binding mode for H2 with gyrase. (A) View of the binding cavity, showing H2 as cyan sticks, bound to the surface of gyrase (4URO). (B) Profile view of H1 ascyan sticks bound in the gorge pocket of gyrase. Key residues for the binding of H1are shown as green sticks. (C) 3D schematic diagram of docking model of H2 showing the hydrogen bonds formed with the gyrase active site.

3.4.1 Drug-likeness and ADMET profiling

The pharmacokinetics and drug-likeness properties of the three hydrazone analogs **SBH**, **H1**, and **H2** were evaluated in silico and their results are mentioned in tables 5 and 6. The three compounds fit the criteria of Lipinski's rule of five with molecular weights below 500g/mol, a number of donor H-bonds below 5, a number of acceptor H-bonds below 10, and a lipophilicity coefficient less than 5,[92] suggesting the biological availability of the three molecules. On the other hand, the solubility of the three compounds in water ranges from excellent for SBH with a logS of -3.92, to moderate for **H1** and **H2** with logS of -5.88 and -

7.30, respectively. Additional screening tests were done for the three analogs in order to characterize their pharmacokinetics, based on several biological parameters like blood-brain barrier penetration (BBB), permeability assay (Caco2), human intestinal absorption (HIA), and cytochrome inhibition. Results of these parameters reveal that **SBH**, **H1**, and **H2** cannot cross the brain membrane, therefore do not present any risk of acting on the central nervous system. In addition, the three molecules present good absorption through biological membranes as shown by Caco2 and HIA parameters, thus promoting their bioavailability as active molecules. Concerning their inhibitory potential against cytochrome P45, **SBH** shows a possible inhibition of cytochrome CYP2C19. Similarly, **H1** and **H2** can have effects on a certain class of cytochrome in particular CYP1A2 and CYP2C19. The analysis of the toxicological behavior of the three compounds; reveals that these molecules have no carcinogenic, mutagenic, or cardiotoxic effect, suggesting their safety for human health.

Table 5. Drug-likeness properties of the three hydrazone analogs SBH, H1, and H2.

	MW g/mol	LogP	Log S	HBA	HBD	TPSA (Å^2)	AMR	Lipinski	Ghose	Veber	Egan	Muegge
SBH	321.18	0.69	-3.92	8	0	136.29	76.42	Yes	Yes	Yes	No	Yes
H1	402.40	2.71	-5.88	5	1	115.49	120.26	Yes	No	Yes	Yes	No
H2	472.88	3.73	-7.30	5	1	115.49	137.81	Yes	No	Yes	No	No

LogP: Lipophilicity; LogS: Water Solubility; HBA: Num. H-bond acceptors; HBD: Num. H-bond donors; TPSA: Topological polar surface area ; AMR: Atom Molar Refractivity

Table 6. ADMET properties of the three hydrazone analogs SBH, H1, and H2.

	BBB	Caco2	HIA	P-gp inhibitor	CYP_{1A2} inhibitor	CYP_{2C19}inhibitor	CYP_{2C9} inhibitor	CYP_{2D6} inhibitor	CYP_{3A4} inhibitor	Ames mutagenesis	Carcinogenicity	hERG_inhibition	H-HT
SBH	No	High	High	No	No	Yes	No	No	No	No	No	No	Yes
H1	No	Medium	Medium	No	Yes	Yes	Yes	No	No	No	No	No	Yes
H2	No	Medium	Medium	No	No	Yes	No	No	No	No	No	No	Yes

BBB: Blood-Brain Barrier; Caco2: Permeability assay; HIA: Human Intestinal Absorption; hERG: human Ether-a-go-go-Related Gene potassium channel; H-HT: Human Hepatotoxicity.

3.4.2 Pharmacophore modeling

The ligand-based pharmacophore modeling approach can be used in complement to molecular docking to optimize the drug development process. This method uses data or features of a set of compounds known to attach a targeted protein in order to predict other compounds with similar features.[93] The promising antibacterial activity of the compounds **H1** and **H2** observed from the in vitro and in silico analyzes, encouraged us to develop a ligand-based pharmacophore model from these two training molecules. The developed pharmacophore query shown in Figure 14 includes combined features selected from the two compounds **H1** and **H2**, which are an acceptor/donor H-bond region and a hydrophobic region. The built pharmacophore model provides a comprehensive tool for gaining a better understanding of current pharmacokinetic properties and can be used to create molecules with improved antibacterial activity.

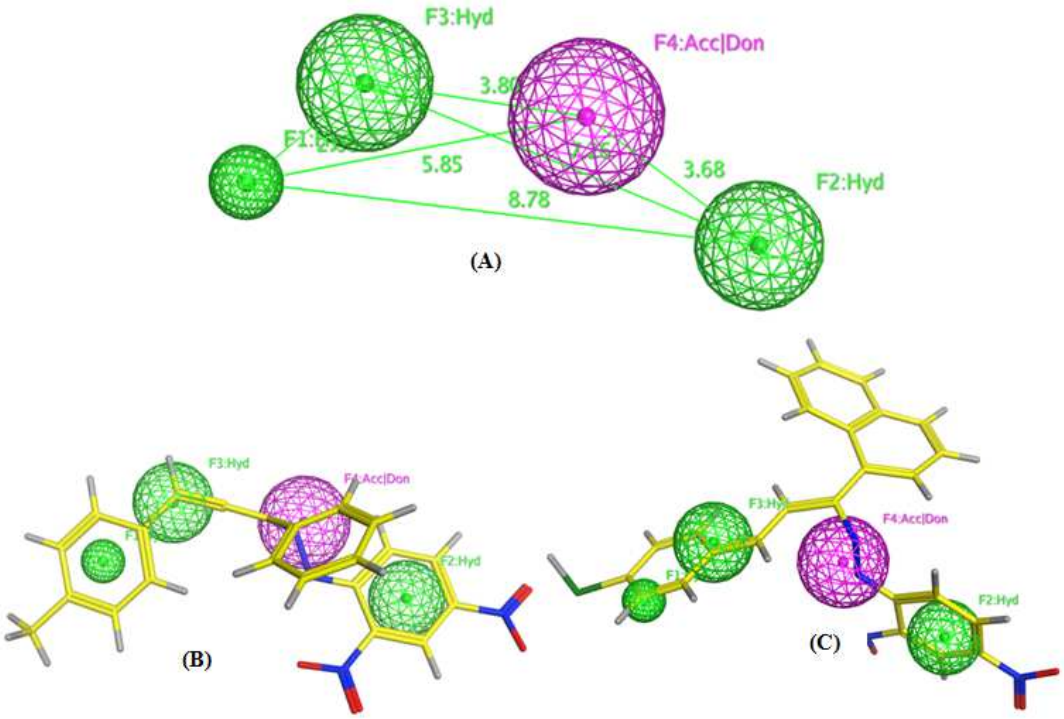

Figure 14. Pharmacophore model and its mapping to representative compounds. (A) The topological features of the model with distances in Angstrom: the magentacontour represents acceptor/donorH-bond (Acc/Don), green contour represents hydrophobic region (Hyd). (B) H1 mapped with the model. (C) H2 mapped with the model.

4 Conclusion

During this work, we were interested in the preparation and the evaluation of the biological potential of 2,4-dinitrophenylhydrazone derivatives **SBH**, **H1** and **H2** in order to study the relationship structure-activity.

The results of the antioxidant activity are in good agreement with the characterized structure and reported spectroscopic investigations of the synthesized compound **SBH**. In fact, this *Schiff* base 2,4-dinitrophenylhydrazone exhibited a free radical scavenging activity rated 68.08% at a concentration of 400 µg/mL, with an IC_{50} = 269.55 µg/mL.

The comparison of the biological properties with the structures of the studied hydrazones, confirms that the antibacterial and antioxidant activities are due respectively to the (*E*)-chalcone and 4-(2-hydrazono)methyl-2-methoxyphenol pharmacophore fragments, respectively.

Furthermore, a theoretical investigation is provided based on geometry optimization of **H1**, **H2**, and **SHB** compounds, is presented. The findings showed for **H2** a considerable enhancement of the electrophilicity, a remarkable decrease in chemical hardness, and an increase in the absolute values of the chemical potentials compared to those of **H1** and **SHB**; predicting the best antibacterial activity correlated with the calculated HOMO and LUMO energies and their gap.

The localization of the spin density relative to the unpaired electron is a good indicator of the N–H or O–H bond-breaking preference. The more the spin density is delocalized, the more the ease of the H-abstraction; thus, the BDEs and the spin densities are strongly related. The obtained BDEs' values put emphasis on good antioxidant potential, particularly for the **SHB** compound corroborating the experimental antioxidant assays.

The Docking study provides a molecular basis for the inhibitory potential of these three compounds towards DNA gyrase. Indeed, the results of this analysis are in accord with those obtained from the in vitro antibacterial activity tests. It can be concluded that the two synthetic compounds **H1** and **H2** possess antibacterial activity by inhibiting DNA gyrase as a potential target.

Supplementary Information (SI)

Schemes S1-S2, Figures S1-S16, and Tables S1-S6 are available as Supplementary Information.

Acknowledgements

The authors are grateful to DGRSDT (Direction Générale de la Recherche Scientifique et du Développement Technologique) for financial support.

Competing interests

The authors declared that there is no conflict of interest.

References

1. Liu W, Ma L, Zhang L, Chen Y, Zhang Q, Zhang H, Zhang W, Zhang C and Zhang W 2022 Two New Phenylhydrazone Derivatives from the Pearl River Estuary Sediment-Derived Streptomyces sp. SCSIO 40020 *Mar. Drugs* 20 449 https://doi.org/10.3390/md20070449

2. Belskaya NP, Dehaen W and Bakulev VA 2010 Synthesis and properties of hydrazones bearing amide, thioamide and amidine functions *Arkivoc* 1 275-332 https://doi.org/10.3998/ark.5550190.0011.108

3. Nikolaevskii A, Kniga O, Khizhan E, Tikhonova G, Vinogradov V and Khizhan A 2012 Antioxidant activity of hydrazones with sterically hindered phenol fragments *Russ. J. Phys. Chem.* 86 1816-1820 https://doi.org/10.1134/S0036024412120205

4. Vicini P, Zani F, Cozzini P and Doytchinova I 2002 Hydrazones of 1, 2-benzisothiazole hydrazides: synthesis, antimicrobial activity and QSAR investigations. *Eur. J. Med. Chem.* 37 553-564 https://doi.org/10.1016/S0223-5234(02)01378-8

5. Zha G-F, Leng J, Darshini N, Shubhavathi T, Vivek H, Asiri AM, Marwani HM, Rakesh K, Mallesha N and Qin H-L 2017 Synthesis, SAR and molecular docking studies of benzo [d] thiazole-hydrazones as potential antibacterial and antifungal agents *Bioorg. Med. Chem. Lett.* 27 3148-3155 https://doi.org/10.1016/j.bmcl.2017.05.032

6. Yildir I, Perçiner H, Sahin MF and Abbasoglu U 1995 Hydrazones of [(2-Benzothiazolylthio) acetyl] hydrazine: Synthesis and Antimicrobial Activity *Arch. Pharm.* 328 547-549 https://doi.org/10.1002/ardp.19953280614

7. Hameed A, al-Rashida M, Uroos M, Abid Ali S and Khan KM 2017 Schiff bases in medicinal chemistry: a patent review (2010-2015) *Expert Opin. Ther. Pat.* 27 63-79 https://doi.org/10.1080/13543776.2017.1252752

8. Maheswari R and Manjula J 2016 Vibrational spectroscopic analysis and molecular docking studies of (E)-4-methoxy-N′-(4-methylbenzylidene) benzohydrazide by DFT J. Manjula *J. Mol. Struct.* 1115 144-155

https://doi.org/10.1016/j.molstruc.2016.02.066
9. Khamaysa OMA, Selatnia I, Zeghache H, Lgaz H, Sid A, Chung I-M, Benahmed M, Gherraf N and Mosset P 2020 Enhanced corrosion inhibition of carbon steel in HCl solution by a newly synthesized hydrazone derivative: Mechanism exploration from electrochemical, XPS, and computational studies *J. Mol. Liq.* 315 113805
https://doi.org/10.1016/j.molliq.2020.113805
10. Khamaysa OMA, Selatnia I, Lgaz H, Sid A, Lee H-S, Zeghache H, Benahmed M, Ali IH and Mosset P 2021 Hydrazone-based green corrosion inhibitors for API grade carbon steel in HCl: Insights from electrochemical, XPS, and computational studies *Colloids Surf., A* 626 127047
https://doi.org/10.1016/j.colsurfa.2021.127047
11. Al Zoubi W 2013 Biological activities of Schiff bases and their complexes: a review of recent works *Int. J. Org. Chem.* 3 73
https://doi.org/10.4236/ijoc.2013.33A008
12. Aggarwal S, Paliwal D, Kaushik D, Gupta GK and Kumar A 2018 Pyrazole Schiff base hybrids as anti-malarial agents: synthesis, in vitro screening and computational study *Comb. Chem. High Throughput Screening* 21 194-203
https://doi.org/10.2174/1386207321666180213092911
13. Sridhar SK, Pandeya SN, Stables JP and Ramesh A 2002 Anticonvulsant activity of hydrazones, Schiff and Mannich bases of isatin derivatives *Eur. J. Pharm. Sci.* 16 129-132
https://doi.org/10.1016/S0928-0987(02)00077-5
14. Xu J, Zhou T, Xu Z-Q, Gu X-N, Wu W-N, Chen H, Wang Y, Jia L, Zhu T-F and Chen R-H 2017 Synthesis, crystal structures and antitumor activities of copper (II) complexes with a 2-acetylpyrazine isonicotinoyl hydrazone ligand *J. Mol. Struct.* 1128 448-454
https://doi.org/10.1016/j.molstruc.2016.09.016
15. Ali SMM, Azad MAK, Jesmin M, Ahsan S, Rahman MM, Khanam JA, Islam MN and Shahriar SMS 2012 In vivo anticancer activity of vanillin semicarbazone *Asian Pac. J. Trop. Biomed.* 2 438-442
https://doi.org/10.1016/S2221-1691(12)60072-0
16. Shockravi A, Sadeghpour M and Olyaei A 2010 Simple and Efficient Procedure for the Synthesis of Symmetrical Bis-Schiff Bases of 5, 5′-Methylenebis (2-aminothiazole) Under Solvent-Free Conditions *Synth. Commun.* 40 2531-2538
https://doi.org/10.1080/00397910903277896
17. Saouli S, Selatnia I, Zouchoune B, Sid A, Zendaoui SM, Bensouici C and Bendeif E-E 2020 Synthesis, spectroscopic characterization, crystal structure, DFT studies and biological activities of new hydrazone derivative: 1-(2, 5-bis ((E)-4-isopropylbenzylidene) cyclopentylidene)-2-(2, 4-dinitrophenyl) hydrazine *J. Mol. Struct.* 1213 128203
https://doi.org/10.1016/j.molstruc.2020.128203
18. Zouchoune B 2020 How the ascorbic acid and hesperidin do improve the biological activities of the cinnamon: Theoretical investigation *Struct. Chem.* 31 2333-2340
https://doi.org/10.1007/s11224-020-01594-w
19. Zouchoune B 2021 Theoretical investigation on the biological activities of ginger and some of its combinations: an overview of the antioxidant activity *Struct. Chem.* 32, 1659-1672
https://doi. org/10.1007/s11224-021-01725-x
20. Dammene Debbih O, Sid A, Bouchene R, Bouacida S, Mazouz W and Gherraf N 2018 Two hydrazones derived from 1-aryl-3-(p-substituted phenyl) prop-2-en-1-one: synthesis, crystal structure, Hirshfeld surface analysis and in vitro biological properties *Acta Crystallogr. C Struct. Chem*. 74 703-714
https://doi.org/10.1107/S2053229618006812
21. Rosca I, Petrovici AR, Brebu M, Stoica I, Minea B and Marangoci N 2016 An original method for producing acetaldehyde and diacetyl by yeast fermentation *Braz. J. Microbiol.* 47 949-954

https://doi.org/10.1016/j.bjm.2016.07.005
22. Humphries RM, Hindler JA, Shaffer K and Campeau SA 2019 Evaluation of ciprofloxacin and levofloxacin disk diffusion and Etest using the 2019 Enterobacteriaceae CLSI breakpoints *J. Clin. Microbiol.* 57 e01797-01718
https://doi.org/10.1128/JCM.01797-18
23. Constantin S, Lupascu FG, Apotrosoaei M, Vasincu IM, Lupascu D, Buron F, Routier S and Profire L 2017 Synthesis and biological evaluation of the new 1, 3-dimethylxanthine derivatives with thiazolidine-4-one scaffold *Chem. Cent. J.* 11 12
https://doi.org/ 10.1186/s13065-017-0241-0
24. Sánchez-Moreno C, Larrauri JA and Saura-Calixto F 1998 A procedure to measure the antiradical efficiency of polyphenols *J. Sci. Food Agric.* 76 270-276
https://doi.org/10.1002/(SICI)1097-0010(199802)76:2<270::AID-JSFA945>3.0.CO;2-9
25. Bentabet N, Boucherit-Otmani Z and Boucherit K 2014 Composition chimique et activité antioxydante d'extraits organiques des racines de Fredolia aretioides de la région de Béchar en Algérie *Phytothérapie* 12 364-371
https://doi.org/10.1007/s10298-014-0834-x
26. ADF2016.01 Version, Theoretical Chemistry, Vrije Universiteit: Amsterdam. The Netherlands, SCM
27. Baerends E, Ellis D and Ros P 1973 Self-consistent molecular Hartree—Fock—Slater calculations I. The computational procedure *Chem. Phys.* 2 41-51
https://doi.org/10.1016/0301-0104(73)80059-X
28. te Velde G and Baerends E 1992 Numerical integration for polyatomic systems *J. Comput. Phys* 99, 84-98
https://doi.org/10.1016/0021-9991(92)90277-6
29. Fonseca Guerra C, Snijders J, Te Velde Gt and Baerends EJ 1998 Towards an order-N DFT method *Theor. Chem. Acc.* 99 391-403
https://doi.org/10.1007/s002140050353
30. Bickelhaupt FM and Baerends EJ 2000 Kohn-Sham density functional theory: predicting and understanding chemistry Rev. Comput. Chem. 15 1-86
https://doi.org/10.1002/9780470125922.ch1
31. Te Velde Gt, Bickelhaupt FM, Baerends EJ, Fonseca Guerra C, van Gisbergen SJ, Snijders JG and Ziegler T 2001 Chemistry with ADF *J. Comput. Chem.* 22 931-967
https://doi.org/10.1002/jcc.1056
32. Vosko SH, Wilk L and Nusair M 1980 Accurate spin-dependent electron liquid correlation energies for local spin density calculations: a critical analysis *Can. J. Phys.* 58 1200-1211
https://doi.org/10.1139/p80-159
33. Becke AD 1993 Becke's three parameter hybrid method using the LYP correlation functional *J. Chem. Phys.* 98 5648-5652
https://doi.org/10.1063/1.464913
34. Lee C, Yang W and Parr RG 1988 Development of the Colle-Salvetti correlation-energy formula into a functional of the electron density *Phys. Rev. B* 37 785
https://doi.org/10.1103/physrevb.37.785
35. Versluis L and Ziegler T 1988 The determination of molecular structures by density functional theory. The evaluation of analytical energy gradients by numerical integration *J. Chem. Phys.* 88 322-328
https://doi.org/10.1063/1.454603
36. Fan L and Ziegler T 1992 Application of density functional theory to infrared absorption intensity calculations on main group molecules *J. Chem. Phys.* 96 9005-9012
https://doi.org/10.1063/1.462258
37. Fan L and Ziegler T 1992 Application of density functional theory to infrared absorption intensity calculations on transition-metal carbonyls *J. Phys. Chem.* 96 6937-6941
https://doi.org/10.1021/j100196a016

38. DiLabio G, Pratt D, LoFaro A and Wright JS 1999 Theoretical study of X− H bond energetics (X= C, N, O, S): Application to substituent effects, gas phase acidities, and redox potentials *J. Phys. Chem.* A 103 1653-1661
https://doi.org/10.1021/jp984369a
39. Feng Y, Liu L, Wang J-T, Huang H and Guo Q-X 2003 Assessment of experimental bond dissociation energies using composite ab initio methods and evaluation of the performances of density functional methods in the calculation of bond dissociation energies *J. Chem. Inf. Comput. Sci.* 43 2005-2013
https://doi.org/10.1021/ci034033k
40. Klamt A and Schüürmann G 1993 COSMO: a new approach to dielectric screening in solvents with explicit expressions for the screening energy and its gradient *J. Chem. Soc., Perkin trans.* 2 799-805
https://doi.org/10.1039/P29930000799
41. Trott O and Olson AJ 2010 AutoDock Vina: improving the speed and accuracy of docking with a new scoring function, efficient optimization, and multithreading *J. Comput. Chem.* 31 455-461
https://doi.org/10.1002/jcc.21334
42. Tai W, Lu T, Yuan H, Wang F, Liu H, Lu S, Leng Y, Zhang W, Jiang Y and Chen Y 2012 Pharmacophore modeling and virtual screening studies to identify new c-Met inhibitors *J. Mol. Model.* 18 3087-3100
https://doi.org/10.1007/s00894-011-1328-5
43. OriginPro 9.0 SR2 software 2013 OriginLab Corporation, Northampton, MA, USA, April 2013
44. Enrique S 2018 MestReNova [software]. Version 12.0.2-20910, Mestrelab Research, Santiago de Compostela, Spain
45. Sundaraganesan N, Kalaichelvan S, Meganathan C, Joshua BD and Cornard J 2008 FT-IR, FT-Raman spectra and ab initio HF and DFT calculations of 4-N, N′-dimethylamino pyridine *Spectrochim. Acta - Part A Mol. Biomol. Spectrosc.* 71 898-906
https://doi.org/10.1016/j.saa.2008.02.016
46. Hamidian K, Irandoust M, Rafiee E and Joshaghani M 2012 Synthesis, Characterization, and Tautomeric Properties of Some Azo-azomethine Compounds *Zeitschrift für Naturforschung B* 67 159-164
https://doi.org/10.1515/znb-2012-0208
47. Yang P, Zhao J, Zhang L, Li L and Zhu Z 2015 Intramolecular hydrogen bonds quench photoluminescence and enhance photocatalytic activity of carbon nanodots *Chem.--Eur. J.* 21 8561-8568
https://doi.org/10.1002/chem.201405088
48. Olszowy M 2019 What is responsible for antioxidant properties of polyphenolic compounds from plants? *Plant Physiol. Biochem.* 144 135-143
https://doi.org/10.1016/j.plaphy.2019.09.039
49. Wang L, Yang Q, Li Y, Wang S, Yang F and Zhao X 2021 How the functional group substitution and solvent effects affect the antioxidant activity of (+)-catechin? *J. Mol. Liq.* 327 114818
https://doi.org/10.1016/j.molliq.2020.114818
50. Masoud MS, Ali AE, Shaker MA and Ghani MA 2005 Solvent and substituent effects on spectroscopical changes of some diazoaminobenzene derivatives *Spectrochim. Acta - Part A Mol. Biomol. Spectrosc.* 61 3102-3107
https://doi.org/10.1016/j.saa.2004.10.043
51. Thavasi V, Bettens RPA and Leong LP 2009 Temperature and solvent effects on radical scavenging ability of phenols *J. Phys. Chem. A* 113 3068-3077
https://doi.org/10.1021/jp806679v
52. Cuvelier M-E, Richard H and Berset C 1992 Comparison of the antioxidative activity of some acid-phenols: structure-activity relationship *Biosci., Biotechnol., Biochem.* 56 324-325

https://doi.org/10.1271/bbb.56.324
53. Subramanian M, Vanangamudi G and Thirunarayanan G 2013 Hydroxyapatite catalyzed aldol condensation: Synthesis, spectral linearity, antimicrobial and insect antifeedant activities of some 2, 5-dimethyl-3-furyl chalcones *Spectrochim. Acta - Part A Mol. Biomol. Spectrosc.* 110 116-123
https://doi.org/10.1016/j.saa.2013.03.023
54. Dusso D, Ramirez C, Parise A, Lanza P, Vera DM, Chesta C, Moyano EL and Akhmedov NG 2019 Synthesis of new cyano-substituted analogues of Tröger's bases from bromo-derivatives. A stereochemical dependence of long-range (nJHH, n= 4, 5, and 6) proton–proton and proton–carbon (nJCH, n= 1, 2, 3, 4, and 5) coupling constants of these compounds *Magn. Reson. Chem.* 57 423-454
https://doi.org/10.1002/mrc.4872
55. Souza MAd, Rodrigues LG, Rocha JE, de Freitas TS, Bandeira PN, Marinho MM, Nunes da Rocha M, Marinho ES, Honorato Barreto AC and Coutinho HDM 2023 Synthesis, structural, characterization, antibacterial and antibiotic modifying activity, ADMET study, molecular docking and dynamics of chalcone (E)-1-(4-aminophenyl)-3-(4-nitrophenyl) prop-2-en-1-one in strains of Staphylococcus aureus carrying NorA and MepA efflux pumps *J. Biomol. Struct. Dyn.* 1-22
https://doi.org/10.1080/07391102.2023.2213777
56. Naili N and Zouchoune B 2018 Structural diversity of homobinuclear transition metal complexes of the phenazine ligand: theoretical investigation *Struct. Chem.* 29 725-739
https://doi.org/10.1007/s11224-017-1064-2
57. Nemdili H, Zouchoune B, Zendaoui MS and Ferhati A 2019 Structural, bonding and redox properties of 34-electron bimetallic complexes and their oxidized 32-and 33-electron and reduced 35-and 36-electron derivatives containing the indenyl fused π-system: A DFT overview *Polyhedron* 160 219-228
https://doi.org/10.1016/j.poly.2018.12.049
58. Farah S, Bouchakri N, Zendaoui S-M, Saillard J-Y and Zouchoune B 2010 Electronic structure of bis-azepine transition-metal complexes: a DFT investigation *J. Mol. Struct. THEOCHEM* 953 143-150
https://doi.org/10.1016/j.theochem.2010.05.019
59. Farah S, Ababsa S, Benhamada N and Zouchoune B 2010 Theoretical investigation of the coordination of dibenzazepine to transition-metal complexes: a DFT study *Polyhedron* 29 2722-2730
https://doi.org/10.1016/j.poly.2010.06.020
60. Bouchakri N, Benmachiche A and Zouchoune B 2011 Bonding analysis and electronic structure of transition metal–benzoquinoline complexes: A theoretical study *Polyhedron* 30 2644-2653
https://doi.org/10.1016/j.poly.2011.07.012
61. Mansouri L and Zouchoune B 2015 Substitution effects and electronic properties of the azo dye (1-phenylazo-2-naphthol) species: a TD-DFT electronic spectra investigation *Can. J. Chem.* 93 509-517
https://doi.org/10.1139/cjc-2014-0436
62. Zouchoune B and Mansouri L 2019 Electronic structure and UV–Vis spectra simulation of square planar Bis (1-(4-methylphenylazo)-2-naphtol)-Transition metal complexes [M (L) 2] x (M= Ni, Pd, Pt, Cu, Ag, and x=− 1, 0,+ 1): DFT and TD-DFT study *Struct. Chem.* 30 691-701
https://doi.org/10.1007/s11224-018-1215-0
63. Zendaoui S-M and Zouchoune B 2016 Coordination chemistry of mixed M (benzene)(cyclopendadienyl) sandwich complexes: electronic properties and bonding analysis *New J. Chem.* 40 2554-2564
https://doi.org/10.1039/c5nj02595h

64. Bensalem N and Zouchoune B 2016 Coordination capabilities of anthracene ligand in binuclear sandwich complexes: DFT investigation *Struct. Chem.* 27 1781-1792
https://doi.org/10.1007/s11224-016-0798-6
65. Wiberg KB 1968 Application of the pople-santry-segal CNDO method to the cyclopropylcarbinyl and cyclobutyl cation and to bicyclobutane *Tetrahedron* 24 1083-1096
https://doi.org/10.1016/0040-4020(68)88057-3
66. Weinhold F and Landis CR 2005 Valency and bonding: a natural bond orbital donor-acceptor perspective *Camb. Univ. Press*
https://doi.org/10.5860/choice.43-4035
67. Weinhold F and Glendening ED 2001 NBO 5.0 program manual: natural bond orbital analysis programs. Theoretical Chemistry Institute and Department of Chemistry, University of Wisconsin, Madison, WI 53706
68. Li X-H, Liu X-R and Zhang X-Z 2011 Molecular structure and vibrational spectra of three substituted 4-thioflavones by density functional theory and ab initio Hartree–Fock calculations *Spectrochim. Acta - Part A Mol. Biomol. Spectrosc.* 78 528-536
https://doi.org/10.1016/j.saa.2010.11.022
69. Padmaja L, Ravikumar C, Sajan D, Hubert Joe I, Jayakumar V, Pettit G and Faurskov Nielsen O 2009 Density functional study on the structural conformations and intramolecular charge transfer from the vibrational spectra of the anticancer drug combretastatin-A2 *J. Raman Spectrosc.* 40 419-428
https://doi.org/10.1002/jrs.2145
70. Roy D, Sarkar U, Chattaraj P, Mitra A, Padmanabhan J, Parthasarathi R, Subramanian V, Van Damme S and Bultinck P 2006 Analyzing toxicity through electrophilicity *Molecular diversity* 10 119-131
https://doi.org/10.1007/s11030-005-9009-x
71. Roy D, Pal N, Mitra A, Bultinck P, Parthasarathi R, Subramanian V and Chattaraj P 2007 An atom counting strategy towards analyzing the biological activity of sex hormones *Eur. J. Med. Chem.* 42 1365-1369
https://doi.org/10.1016/j.ejmech.2007.01.028
72. Pearson RG 1987 Recent advances in the concept of hard and soft acids and bases *J. Chem. Educ.* 64 561
https://doi.org/10.1021/ed064p561
73. Parr RG and Yang W 1989 Density-functional theory of atoms and molecules Oxford *Univ. Press, ed: Oxford*
https://doi.org/10.1002/qua.560470107
74. Parr RG, Szentpaly LV and Liu S 1999 Electrophilicity Index *J. Am. Chem. Soc.* 121 1922-1924
https://doi.org/10.1021/ja983494x
75. Chattaraj PK, Maiti B and Sarkar U 2003 Philicity: a unified treatment of chemical reactivity and selectivity *J. Phys. Chem. A* 107 4973-4975
https://doi.org/10.1021/jp034707u
76. Chattaraj PK, Sarkar U and Roy DR 2006 Electrophilicity index *Chem. Rev.* 106 2065–2091
https://doi.org/10.1021/cr040109f
77. Dan W and Dai J 2020 Recent developments of chalcones as potential antibacterial agents in medicinal chemistry *Eur. J. Med. Chem.* 187 111980
https://doi.org/10.1016/j.ejmech.2019.111980
78. Farhadi F, Khameneh B, Iranshahi M and Iranshahy M 2019 Antibacterial activity of flavonoids and their structure–activity relationship: An update review *Phytotherapy Research* 33 13-40
https://doi.org/10.1002/ptr.6208
79. Nowakowska Z, Kędzia B and Schroeder G 2008 Synthesis, physicochemical properties and antimicrobial evaluation of new (E)-chalcones *Eur. J. Med. Chem.* 43 707-713

https://doi.org/10.1016/j.ejmech.2007.05.006
80. Nowakowska Z 2007 A review of anti-infective and anti-inflammatory chalcones *Eur. J. Med. Chem.* 42 125-137
https://doi.org/10.1016/j.ejmech.2006.09.019
81. Chen J, Yang J, Ma L, Li J, Shahzad N and Kim CK 2020 Structure-antioxidant activity relationship of methoxy, phenolic hydroxyl, and carboxylic acid groups of phenolic acids *Sci. Rep.* 10 1-9
https://doi.org/10.1038/s41598-020-59451-z
82. Ouyang X, Li X, Liu J, Liu Y, Xie Y, Du Z, Xie H, Chen B, Lu W and Chen D 2020 Structure–activity relationship and mechanism of four monostilbenes with respect to ferroptosis inhibition *RSC Adv.* 10 31171-31179
https://doi.org/10.1039/D0RA04896H
83. Wright JS, Johnson ER and DiLabio GA 2001 Predicting the activity of phenolic antioxidants: theoretical method, analysis of substituent effects, and application to major families of antioxidants *J. Am. Chem. Soc.* 123 1173-1183
https://doi.org/10.1021/ja002455u
84. Litwinienko G and Ingold K 2003 Abnormal solvent effects on hydrogen atom abstractions. 1. The reactions of phenols with 2, 2-diphenyl-1-picrylhydrazyl (dpph•) in alcohols. *J. Org. Chem.* 68 3433-3438
https://doi.org/10.1021/jo026917t
85. Leopoldini M, Marino T, Russo N and Toscano M 2004 Antioxidant properties of phenolic compounds: H-atom versus electron transfer mechanism *J. Phys. Chem. A* 108 4916-4922
https://doi.org/10.1021/jp037247d
86. Leopoldini M, Marino T, Russo N and Toscano M 2004 Density functional computations of the energetic and spectroscopic parameters of quercetin and its radicals in the gas phase and in solvent. *Theor. Chem. Acc.* 111 210-216
https://doi.org/10.1007/s00214-003-0544-1
87. Leopoldini M, Russo N, Chiodo S and Toscano M 2006 Iron chelation by the powerful antioxidant flavonoid quercetin *J. Agric. Food Chem.* 54 6343-6351
https://doi.org/10.1021/jf060986h
88. Peerannawar S, Horton W, Kokel A, Török F, Török M and Török B 2017 Theoretical and experimental analysis of the antioxidant features of diarylhydrazones *Struct. Chem.* 28 391-402
https://doi .org/10.1007/s11224-016-0867-x
89. Coleman JP and Smith CJ 2014 Microbial Nucleic Acid and Protein Synthesis *Reference Module Biomed. Sci.*
https://doi.org/10.1016/B978-0-12-801238- 3.05147-3
90. Spížek J, Novotná J, Řezanka T and Demain AL 2010 Do we need new antibiotics? The search for new targets and new compounds *J. Ind. Microbiol. Biotechnol.* 37 1241-1248
https://doi.org/10.1007/s10295-010-0849-8
91. Clark DE 2008 What has virtual screening ever done for drug discovery? *Expert Opin. Drug Discov.* 3 841-851
https://doi.org/10.1517/17460441.3.8.841
92. Lipinski CA, Lombardo F, Dominy BW and Feeney PJ 1997 Experimental and computational approaches to estimate solubility and permeability in drug discovery and development settings *Adv. Drug Delivery Rev.* 23 3-25
https://doi.org/10.1016/j.addr.2012.09.019
93. Khedkar SA, Malde AK, Coutinho EC and Srivastava S 2007 Pharmacophore modeling in drug discovery and development: an overview *Med. Chem.* 3 187-197
https://doi.org/10.2174/157340607780059521